Design and Adaptation of Electrohydrodynamic Lens for Stabilizing of Electrohydrodynamic Printing Using Silver Nanocolloid Jet

Yunsoo Shin

The Graduate School

Yonsei University

Department of Mechanical Engineering

Design and Adaptation of Electrohydrodynamic Lens for Stabilizing of Electrohydrodynamic Printing Using Silver Nanocolloid Jet

A Masters Thesis

Submitted to the Department of Mechanical Engineering

and the Graduate School of Yonsei University

in partial fulfillment of

the requirements for the degree of

Master of Science in Mechanical Engineering

Yunsoo Shin

July 2007

This certifies that the master's thesis of Yunsoo Shin is approved.

_____

[Thesis Supervisor: Jungho Hwang]

_____

[Taeu Yu: Thesis Committee Member #1]

_____

[Soonho Song: Thesis Committee Member #2]

The Graduate School

Yonsei University

July 2007

DEDICATED TO MY PARENTS, BROTHER

AND

SPECIAL THANKS FOR EVERYONE TO SUPPORT ME

Contents

Contents ---------- **i**

List of Figures ---------- **iv**

List of Tables ---------- **viii**

Abstract ---------- **ix**

1. Introduction ---------- **1**

1.1 Competing technologies ---------- 1

1.2 Electrohydrodynamic atomization in the cone-jet mode ---------- 8

2. Background & Theory ---------- **11**

2.1 History of cone-jet mode of EHD spraying ---------- 11

2.2 The definition of cone-jet mode and nanocolloid jet ---------- 14

2.3 Pin-Pin type EHD nanocolloid jet printing system ---------- 15

2.4 Problems of Pin-Pin type EHD nanocolloid jet printing system ----- 18

3. Feasibility test of Pin-Lens type ---------- 19

3.1 Idea of Pin-Lens type system ---------- 19

3.2 Experimental setting ---------- 21

3.3 Results ---------- 23

3.4 Objectives ---------- 26

4. Physical modeling of EHD lens for focusing and stabilizing ---------- 27

4.1 Introduction ---------- 27

4.2 Design of electrohydrodynamic lens ---------- 28

4.3 Simulation results ---------- 30

4.4 Calculation results ---------- 43

5. Patterning of EHD nanocolloid jet by using the EHD lens ---------- 60

5.1 Experimental setting ---------- 60

5.2 Results ---------- 62

6. Discussion & Conclusions ---------- 66

▪ Reference ---------- 67

▪ Summary in Korean (국문요약) ---------- 73

List of Figures

Figure 1-1 Throughput vs. Resolution of different kind of printing processes

Figure 1-2 Flexographic Printing Process

Figure 1-3 Diagram of the microcontact printing process

Figure 1-4 Gravure printing process

Figure 1-5 Offset lithographic printing

Figure 1-6 Tech-tree of Inkjet technology

Figure 1-7 Inkjet deposition mechanisms. Thermal(left), Piezo(Right)

Figure 1-8 Modes of electrospray

Figure 1-9 Captured pictures of electrospray modes

Figure 2-1 Different regions of cone-jet mode

Figure 2-2 Schematic forces in the liquid cone

Figure 2-3 Schematic of Pin-Pin type printing system

Figure 2-4 Square-shape pattern

Figure 3-1 Idea of printhead design

Figure 3-2 Multiple field electrospinning

Figure 3-3 Schematic diagram of experimental setup

Figure 3-4 Magnified image of rectangular

Figure 3-5 Type I lens

Figure 3-6 Patterned image by Type I lens

Figure 3-7 Captured picture of EHD nanocolloid jet

Figure 4-1 Design of electrohydrodynamic lens

Figure 4-2 Maxwell analysis of electrohydrodynamic lens

Figure 4-3 Maxwell analysis of electrohydrodynamic lens (corner parts of magnified)

Figure 4-4(a) COMSOL analysis of electrohydrodynamic Type I lens (overall)
Figure 4-4(b) COMSOL analysis of electrohydrodynamic Type II lens (overall)
Figure 4-4(c) COMSOL analysis of electrohydrodynamic Type III lens (overall)
Figure 4-4(d) COMSOL analysis of electrohydrodynamic Type IV lens (overall)
Figure 4-5(a) COMSOL analysis of electrohydrodynamic Type I lens (Contour 40)
Figure 4-5(b) COMSOL analysis of electrohydrodynamic Type II lens (Contour 40)
Figure 4-5(c) COMSOL analysis of electrohydrodynamic Type III lens (Contour 40)
Figure 4-5(d) COMSOL analysis of electrohydrodynamic Type IV lens (Contour 40)
Figure 4-6(a) COMSOL analysis of electrohydrodynamic Type I lens (Contour 20)
Figure 4-6(b) COMSOL analysis of electrohydrodynamic Type II lens (Contour 20)
Figure 4-6(c) COMSOL analysis of electrohydrodynamic Type III lens (Contour 20)
Figure 4-6(d) COMSOL analysis of electrohydrodynamic Type IV lens (Contour 20)
Figure 4-7(a) COMSOL analysis of electrohydrodynamic Type I lens
(Contour 40 & Stream line)
Figure 4-7(b) COMSOL analysis of electrohydrodynamic Type II lens
(Contour 40 & Stream line)
Figure 4-7(c) COMSOL analysis of electrohydrodynamic Type III lens
(Contour 40 & Stream line)
Figure 4-7(d) COMSOL analysis of electrohydrodynamic Type IV lens
(Contour 40 & Stream line)
Figure 4-8(a) COMSOL analysis of electrohydrodynamic Type III lens
(Contour 40 & Stream line)
Figure 4-8(b) COMSOL analysis of electrohydrodynamic Type III-a lens
(Contour 40 & Stream line)

Figure 4-9(a) Diagram of Data line

Figure 4-9(b) Diagram of Data line

Figure 4-10(a) Diagram of Data line without lens

Figure 4-10(b) Diagram of Data line Type I lens

Figure 4-10(c) Diagram of Data line Type II lens

Figure 4-10(d) Diagram of Data line Type III lens

Figure 4-10(e) Diagram of Data line Type IV lens

Figure 4-11(a) Graph of Line 1 (Upper 0.1mm at substrate)

Figure 4-11(b) Graph of Line 2 (Upper 1.0mm at substrate)

Figure 4-11(c) Graph of Line 3 (Upper 1.9mm at substrate)

Figure 4-12(a) Matrix calculation of Type I lens at Line 3
(Fixed Z axial ; 1.9mm to substrate)

Figure 4-12(b) Matrix calculation of Type II lens at Line 3
(Fixed Z axial ; 1.9mm to substrate)

Figure 4-12(c) Matrix calculation of Type III lens at Line 3
(Fixed Z axial ; 1.9mm to substrate)

Figure 4-12(d) Matrix calculation of Type IV lens at Line 3
(Fixed Z axial ; 1.9mm to substrate)

Figure 4-13(a) Matrix calculation of Type I lens at Line 1
(Fixed Z axial ; 0.1mm to substrate)

Figure 4-13(b) Matrix calculation of Type II lens at Line 1
(Fixed Z axial ; 0.1mm to substrate)

Figure 4-13(c) Matrix calculation of Type III lens at Line 1
(Fixed Z axial ; 0.1mm to substrate)

Figure 4-13(d) Matrix calculation of Type IV lens at Line 1
(Fixed Z axial ; 0.1mm to substrate)
Figure 4-14(a) Matrix calculation of Type I lens (Fixed X axial)
Figure 4-14(b) Matrix calculation of Type II lens (Fixed X axial)
Figure 4-14(c) Matrix calculation of Type III lens (Fixed X axial)
Figure 4-14(d) Matrix calculation of Type IV lens (Fixed X axial)
Figure 4-15(a) Matrix calculation of Type I lens (Fixed X axial)
Figure 4-15(b) Matrix calculation of Type II lens (Fixed X axial)
Figure 4-15(c) Matrix calculation of Type III lens (Fixed X axial)
Figure 4-15(d) Matrix calculation of Type IV lens (Fixed X axial)
Figure 5-1 Experimental setting
Figure 5-2 Diagram of Substrate (FR-4)
Figure 5-3 Substrate (FR-4)
Figure 5-4(a) Pattern result of Type II lens (Photo paper)
Figure 5-4(b) Pattern result of Type III lens (Photo paper)
Figure 5-5 Comparison of pattern result by using Type I lens
(FR4; One-side coating of Cu)
Figure 5-6 Pattern result by using Type I lens
(FR4; without Cu coating)
Figure 5-7 Pattern result by using Type I lens (FR4; Double-faced coating of Cu)

List of Table

Table 1-1 Printing process parameter comparison

Table 3-1 Geometric of electrohydrodynamic lens (unit : mm)

Table 3-2 Experimental Conditions & Pattern width

Table 4-1 Geometric of electrohydrodynamic lens (unit : mm)

Abstract

Design and Adaptation of Electrohydrodynamic Lens for Stabilizing of Electrohydrodynamic Printing Using the Silver Nanocolloid Jet

Electrohydrodynamic printing (EHDP) is one of the novel printing methods for direct writing technology. As a direct write technology, the electrohydrodynamic nanocolloid jet printing (NCJP) of silver nanoparticles by using a electrohydrodynamic (EHD) lens. In this paper, Pin-Lens types manufactured without ground pin that examples of 2-dimensional patterning were printed by using the electrohydrodynamic NCJP. Four types of electrohydrodynamic lens showed physical modeling and a spiral-type inductor was printed to demonstrate the feasibility of the electrohydrodynamic nanocolloid jet printing as a fabrication process. Then, complex geometries having square and various patterns were also printed. Pin-Lens type experiment easily set up the alignment between nozzle and ground how to design of electrohydrodynamic lens. The answer is mix up the guide ring and ground electrode. Secondly important object is focusing. Experiment of Pin-Lens type need to gain more fine patterns than Pin-Pin type. Third important object is that we will be to gain the stabilizing electro-hydrodynamic nanocolloid jet How to design of electrohydrodynamic lens, through a modified geometry of lens. So this thesis tries that various geometry of electrohydrodynamic lens analysis by using the commercial solver package. And we compare pattern result with physical modeling result.

Two dimensional electric field strengths of four types of lens calculate between the nozzle and the lens. The dotted lines in picture indicated the degree of dispersion of

electric field strength. When the Type IV lens was used, the electric field strength was concentrated near the center of the lens and thus narrow electric fields were generated at the end of the lens. Consequently, it is expected that the jet break up would be minimized when Type IV lens used.

Patterns of silver nanoparticles were obtained by using the various electrohydrodynamic lenses in electrohydrodynamic printing. The pattern width measured by using the Type I lens was about 150 μm. When the Type II and III were used, the pattern widths measured were about 100 μm and 80 μm. When the Type IV lens was used, the simulation results showed that the electric field strength was concentrated near the center of the lens and thus narrow electric fields were generated at the end of the lens. Pin-Lens type of electrohydrodynamic system proves to possible electrohydrodynamic nanocolloid jet printing and Lens do a role between electrode and guide ring at Pin-Pin type. As previously explained, the more electric field strength is higher, the more repulsive force is higher. Because Type IV lens is to generate highest electric field strength, radial force of outside effect is very little. Data of Each line gained by the Maxwell, as show likely physical modeling result, which arrange by Origin as form of Matrix 3-dimension.. Because low rough of graph face is little effect of radial force, these graphs explain about stabilization.

Keyword : Electrohydrodynamic printing, Electrohydrodynamic lens, Nanocolloid jet printing, Silver, Conductive line, Printing, Patterning

1. Introduction

1.1 Competing technologies

Direct write technology is the most recent and novel approaches of forming a fine pattern whose line width ranges from the meso to the nanoscales. The term direct write refers to any technique or process capable of depositing, dispensing, or processing different types of materials over various surfaces following a preset pattern or layout. Direct-write technologies are subset of the larger area of rapid prototyping and deal with coatings for structures considered to be two-dimensional in nature. The ability to deposit and pattern different thin-film materials is inherent to the fabrication of components and system such as those found in electronic devices, sensors, MEMS, etc. The trend toward miniaturization has been led by developments in lithography techniques, equipment, and resists materials. But with increased capabilities come limited flexibility as well as increased complexity, time, and cost.

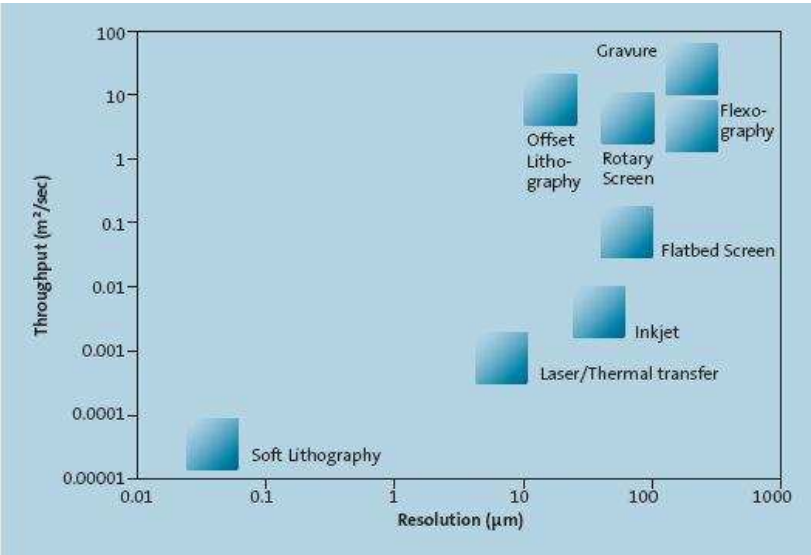

Figure 1-1 Throughput vs. Resolution of different kind of printing processes

In Printed electronics, there are three major types of considerations for determining the printing process used. Techniques are chosen based upon their suitability for printing the desired materials (viscoelastic properties), as well as by their capability to print the desired feature sizes (lateral resolution, ink thickness, surface uniformity) required by the device. Economic considerations such as process throughput are also important specifications for the major printing processes used in electronics are shown in Table 1-1[a]. As can be seen in Figure 1-1[b], lateral resolution (essentially, the size of the smallest feature that can be printed), is related to the throughput. The printing processes with the highest resolution capability are also generally those with the lowest throughput (and vice versa). The techniques having a throughput > $1m^2$/sec, are known as "high volume" printing processes. These high volume printing process are highly desirable to enable the lowest cost production.

Table 1-1 Printing process parameter comparison

	Physical Master(Analog)						**No Physical Master (Digital, NIP)**	
	Relief				No Relief			
	Raised		Lowered					
	Flexo-graphy	Soft Lithography	Gravure	Pad	Offset Lithography	screen	Ink-jet	Thermal/ Ablation
Lateral Resolution(μm)	75	0.03	75	20	10-50	30	20-50	5
Ink Thickness(μm)	3-8	Monolayer	2-5	4-6	< 2.5	100	~0.1	<1
Ink viscosity (mPas)	50-500		50-200	>50	20,000-100,000	500~ 50,000	<20	N/A
Throughput (m^2/sec)	10	1.E-05	60	0.1	20	<10	0.01	0.002

[a] Source : Printed Electronics Consulting

[b] This table is a compilation of best individual values for graphics applications, which were obtained from various manufacturers specifications and other published reports. These specifications should be considered as only approximate upper limits. Actual values that can be achieved for a particular system will depend upon many other factors. Source : Printed Electronics Consulting

Flexography

The principles of flexographic printing are shown diagrammatically in Figure 1-2[c]. In the normal implementation (also known as “two roll”), ink is transferred from the ink pan via a fountain roll to the anilox roll. The anilox roll controls the amount of ink that is transferred to the printing plate. The anilox roll consists of a number of small cells that are engraved into the surface of the roll. Different anilox rolls are available that contain different size cell and cell volumes The raised areas on the printing plate pick up the ink from the anilox roll as shown in Figure 1-2, and transfer it to the substrate.

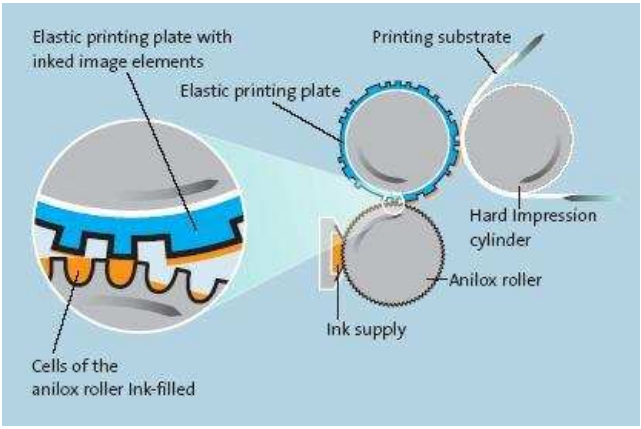

Figure 1-2 Flexographic Printing Process

Soft-Lithography

The most common soft lithography process is called Micro Contact Printing (μCP). Figure 1-3[d] illustrates how the μCP process is performed. First, a mater is created using micro-fabrication processes. Second, the liquid prepolymer is applied to the surface of the master. Third the prepolymer is cured (by heating), and removed form

[c] Source : VDMA
[d] Source : VDMA

the master. Now, ink needs to be applied to the surface of the stamp. This can be done by either applying the ink direction to the stamp (4) or by using and ink pad (5). Most often, the ink used are molecules which form self assembled monolayer (typically thiols) on the surface (typically gold), Sixth, the stamp is brought into contact with the surface to be patterned. Seventh, upon removal of the stamp, a self assembled monolayer (SAM) of ink is formed on the substrate surface. Finally, this SAM is used as an etch resist to selectively etch the underlying substrate surface.

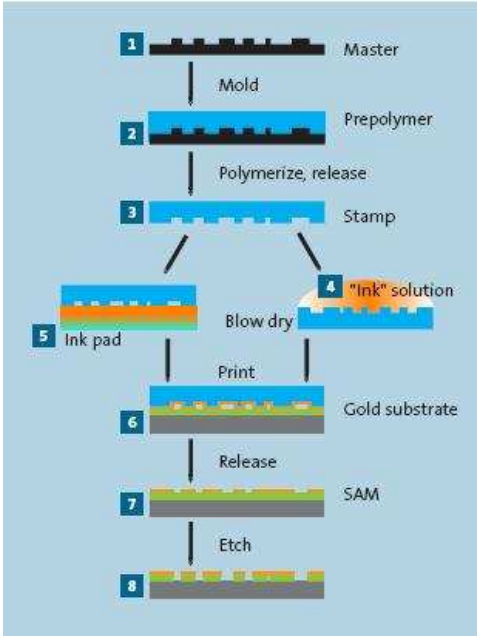

Figure 1-3 Diagram of the microcontact printing process

Gravure

The gravure printing process is shown schematically in Figure 1-4. It is one of the highest volume printing processes, and often used commercially to produce high quality graphic materials, for example magazines. It is one of the few printing process

that can be used to deposit different amounts of material in different locations. Due to the nature of the engraved pits, the edges of printed features may not be smooth and straight.

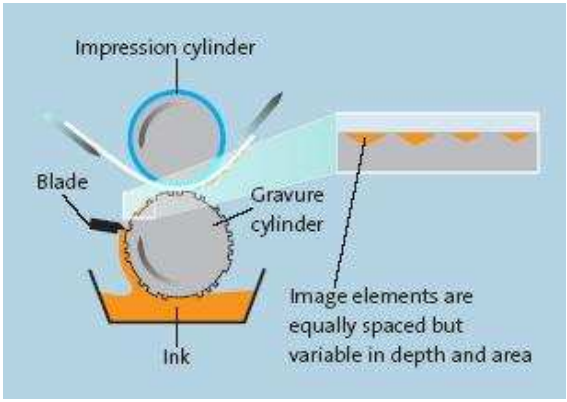

Figure 1-4 Gravure printing process (Source : VDMA)

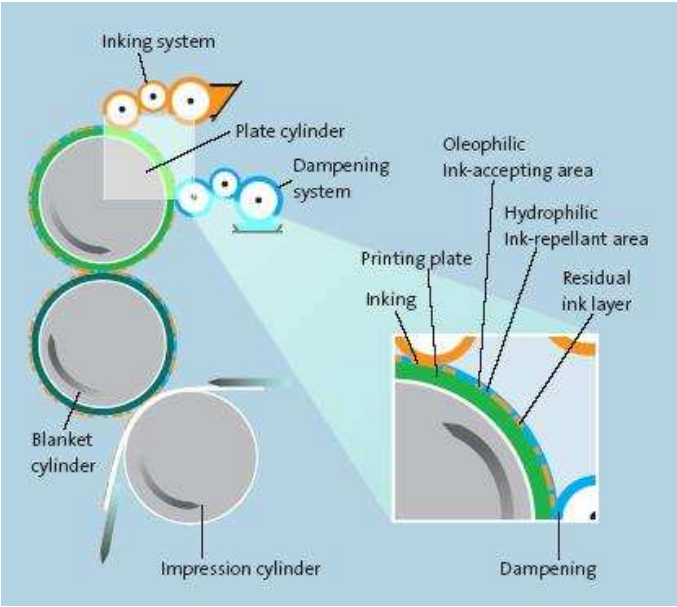

Figure 1-5 Offset lithographic printing (Source : VDMA)

Offset Lithography

Offset lithography is one of the most common printing processes. As described above, it works based on the principle of a difference in surface energy (wetting) of the printing plate (Figure 1-5). Normally two solutions are applied to the plate simultaneously – an ink solution, and an aqueous (water based) fountain solution. The ink sticks to the image areas of the plate, and the fountain solution wets the non image areas. Another version of offset lithography uses special silicone printing plates which do not require the fountain solution. This is known as waterless lithography. The term offset comes from the fact that the ink is transferred from the plate to an intermediate and then to the substrate. The intermediate cylinder is known as the offset cylinder.

Ink-jet

In recent years, Ink-jet printing has been receiving growing interest as a method to deposit functional materials, as opposed to the more conventional graphics applications. Ink-jet printing is particularly good for the deposition of small amount of materials that have specific electrical, optical, chemical, biological, or structural functionalities onto well defined locations on a substrate. The materials deposited can be soluble liquids, dispersions of small (or nano) particles, melts or blends. Some types of functional molecules such as polymers or large bio-molecules can not be deposited by the conventional vacuum deposition techniques, and need to be deposited using a solution based technique. As can be shown in Figure 1-6, a number of manufacturers now produce print heads that designed specifically for printing functional materials. There are two primary mechanisms for ejecting drops from an ink-jet nozzle. In thermal ink-jet, a small portion of the ink solvent is evaporated, forcing ink out of the nozzle in

piezoelectric ink-jet, a voltage is applied to a piezoelectric material which caused it to change its shape (expand), thereby forcing ink out of the nozzle (Figure 1-7)

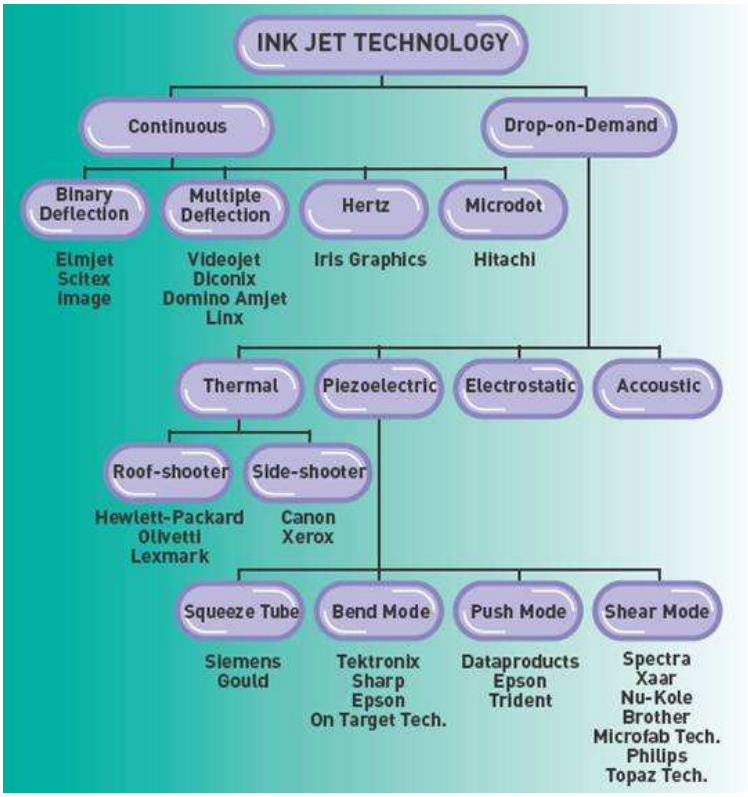

Figure 1-6 Tech-tree of Ink-Jet Technology

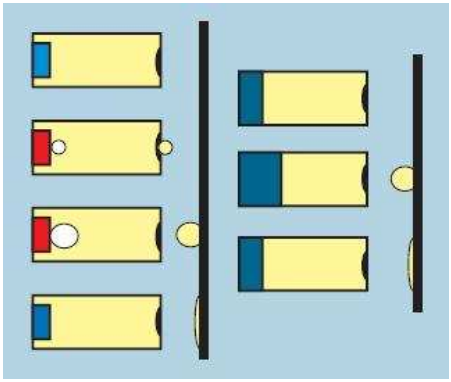

Figure 1-7 Inkjet deposition mechanisms. Thermal(left), Piezo(right)

1.2 Electrohydrodynamic atomization in the cone-jet mode

Electrohydrodynamic atomization, also called electrospraying, refers to a process where a liquid jet breaks up into droplets under influence of electrical forces. However, a liquid jet will also break up into droplets without any electric force present. Depending on the strength of the electric stresses in the liquid surface relative to the surface tension stress, and the kinetic energy of liquid jet leaving the nozzle, different spraying modes will be obtained.

One of these spraying modes is the cone-jet mode, sometimes referred to as the Taylor Cone. In this mode, a liquid is pumped through a nozzle at a low flow rat. An electric field is applied over the nozzle and some counter electrode. This electric field induces a surface charge in the growing droplet at the nozzle. Due to this surface charge, and due to the electric field, and electric stress is created in the liquid surface. If the electric field, and the liquid flow rate are in the appropriate range, then this electric stress will overcome the surface tension stress. In that case, the electric stresses transform the droplet into a conical shape. The tangential electric field accelerates the charge carriers at the liquid surface toward the cone apex. In a liquid, the charge carriers are mainly ions. These ions collide with the surrounding liquid molecules. This results in an acceleration of the surrounding liquid. As a result, a thin liquid jet emerges at the cone apex. This jet can break up into a number of main droplets with a narrow size distribution, and a number of smaller secondary droplet and satellites, Cloupeau and Prunet Forch (1989), Gomez and Tang (1994), Chen et al. (1995). The number of secondary droplets can be of the same order of magnitude as the number of main droplets. However, the total volume of these secondary droplets is much smaller than the volume of main droplets. Due to the excess of surface charge in the liquid

cone and jet, the droplets are highly charged. The droplet size and droplet charge depend mainly on the liquid flow rate and on liquid properties like density, viscosity, conductivity, electrical permittivity, and surface tension. Depending on the liquid properties, the main droplet size produced ranges from nanometers with production frequencies in the order of 10^9Hz to hundreds of micrometers with production frequencies of about 10^4Hz. Small droplets are found at the edge of the spray, while large droplets are found in the spray center, among others Gañán-Calvo et al.(1994). This makes separation of the main droplets from the smaller secondary droplets possible, and a really monodisperse spray can be reached. In that case droplet fission can take place. This effect changes the droplet size distribution. Figure 1-8 shows modes of electrohydrodynamic spraying according to electrical potential.

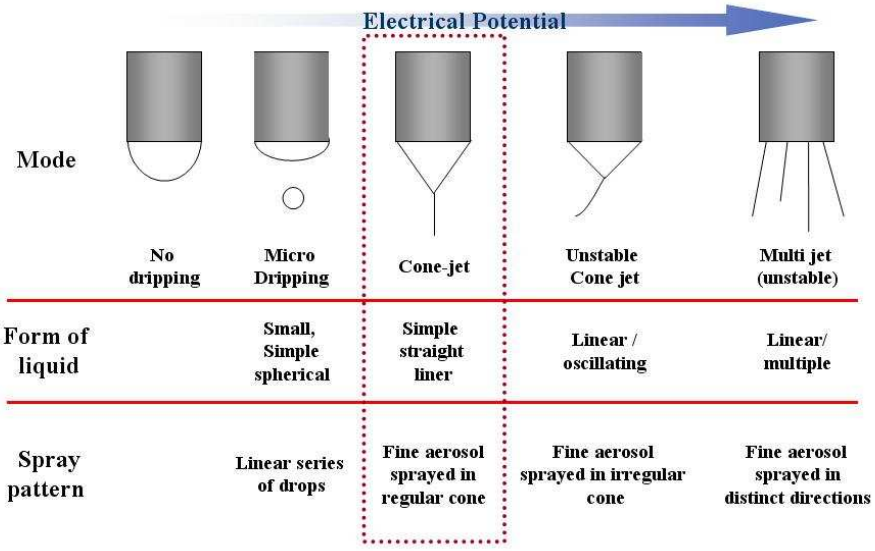

Figure 1-8 Modes of electrospay

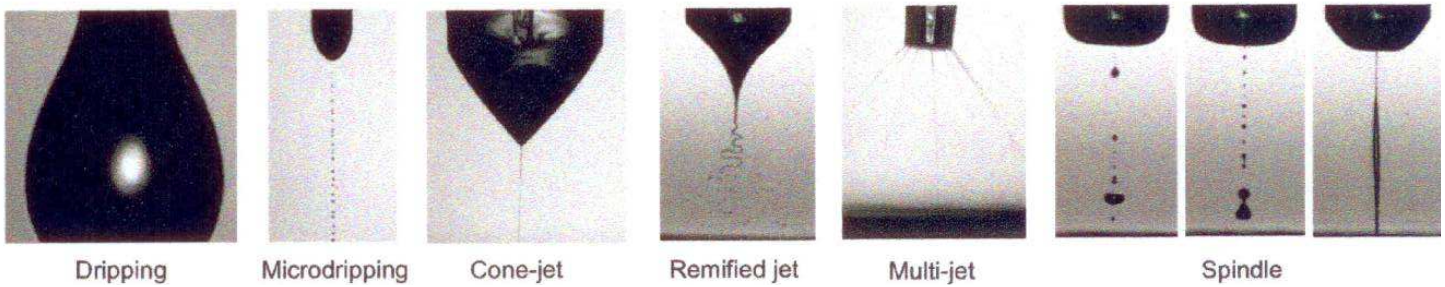

Figure 1-9 Captured pictures of eletrospaying modes

2. Background & Theory

2.1 History of cone-jet mode of EHD spraying

Electrohydrodynamic atomization in the cone-jet mode has been studied for many years now. The phenomenon was first mentioned in 'De Magnete' by William Gilbert in 1600. He observed that a piece of amber, held at a suitable distance, attracts spherical droplets lying on a dry surface, and draws them up into cones. However, it was Zeleny (1914, 1915, 1917), who gave the first solid scientific description of the process. After Vonnegut and Neubauer (1952) rediscovered this phenomenon, many people have contributed to the understanding of Electrohydrodynamic atomization in the cone-jet mode.

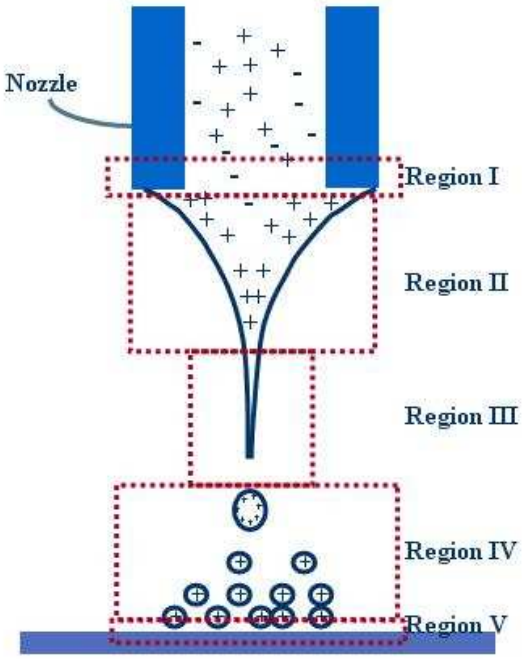

Figure 2-1 Different regions of cone-jet mode

Electrohydrodynamic atomization in the cone-jet mode has to be described by at least five different regions. Figure 2-1 shows the five different regions. The first process, which has region I and region II, is the acceleration of the liquid in the liquid cone. Based on the work of Gañán-Calvo et al. (1997), Fernández de la Mora and Loscertales (1994), and many other people, the following description of this acceleration can be given. The electric field induces a free surface charge in the cone surface. In a liquid, charge is mainly transported by ions. So, the free charge at the liquid surface mainly consists of ions. Due to this surface charge, the normal electric field inside the liquid is small compared to the normal field outside the liquid. This acceleration process and the shape of the liquid cone are a result of the balance of the liquid pressure, liquid surface tension, gravity and electric stresses in the liquid surface, and of the inertia and viscosity of the liquid. Figure 2-2 shows the processes that play a role in the liquid cone. Taylor (1964) was the first to describe the balance between the surface tension stress and the normal electrical stress in a liquid cone.

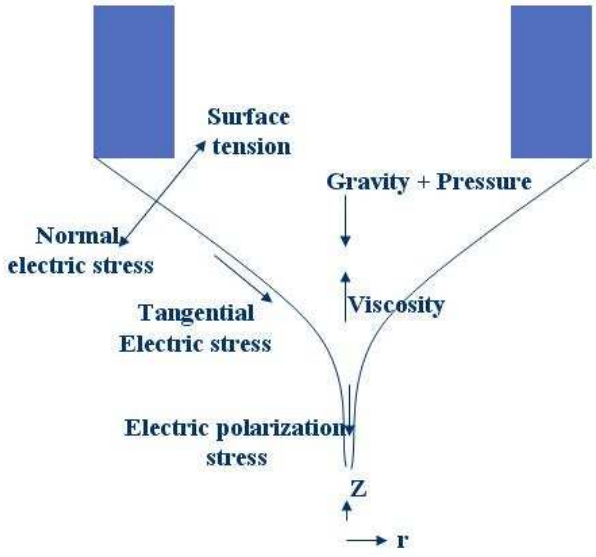

Figure 2-2 Schematic forces in the liquid cone

The second process, which has region III and region IV, is the break-up of the jet into droplets. The jet emerging at the cone apex, breaks often up into a bimodal size distribution. This bimodal size distribution occurs because the jet breaks up into main droplet with a narrow size distribution, and a number of smaller secondary droplets. The break-up of a jet has been studied by many people. For instance, Rayleigh (1878) and Weber (1931) have presented theories to predict the growth rate of varicose instabilities on a liquid jet.

The third process is deposition mechanism of liquid jet in electrohydrodynamic printing. This mechanism of process tries to study and research at present. The special feature and characteristic of cone-jet mode of electrohydrodynamic spraying have attracted many researchers. Taylor calculated analytically a conical shape, which balanced the surface tension and the electrical normal stress with an inviscid liquid. The inclined angle was 49.3°.

$$V = \frac{2H}{L}\sqrt{\left(2\pi r\gamma\cos\phi + W - \pi r^2\Delta \mathrm{p}\right)\left(\ln\left(\frac{2L}{r}\right) - \frac{3}{2}\right)} \tag{1}$$

Fernández et al. (1990) provided scaling laws for jet diameter based on dimensional analysis of all parameters involved in the electrohydrodynamic spraying.

$$d_j \sim \left(\frac{\rho Q^2}{\gamma}\right)^{\frac{1}{3}} \tag{2}$$

Gañán-Calvo (1997) provided scaling law for the generated droplet size and compared with the experimental results. At equation (2), d_j is the jet diameter, Q is flow rate, ρ is density, γ is surface tension, K is conductivity, and ε_0 is vacuum permittivity.

$$d_d = 2.268^{-\frac{2}{3}} Q^{\frac{1}{2}} \left(\frac{\rho \varepsilon_0}{\gamma K} \right)^{\frac{1}{6}} \tag{3}$$

$$d_j \sim \left(\frac{Q \varepsilon \varepsilon_0}{K} \right)^{\frac{1}{3}} \tag{4}$$

Chen and Pui (1997) generated with liquids of different relative permittivity and compared the scaling laws (eq. (3), (4)) with their results. Hartman et al. (1999, 2000) studied the break-up phenomenon of electrically driven liquid jet and developed the Calvo's scaling laws.

$$d_d \sim \left(\frac{\rho \varepsilon_0 Q^3}{\gamma K} \right)^{\frac{1}{6}} \tag{5}$$

$$l = \frac{\mu}{\omega} \ln \left(\frac{a}{\delta_o} \right) \tag{6}$$

Hak Fei Poon (2002) studied the calculate equation of Jet length before the break-up of jet. Li (2006) investigated the spraying phenomenon with pulse bias voltages and Chen et al. (2006) provided scaling laws for drop formation under pulse electrohydrodynamic spraying. At equation (6), l is jet length, μ is viscosity, ω is maximum disturbance growth rate, a and δ_0 are radius of the object and initial disturbance of the jet.

2.2 The definition of cone-jet mode and nanocolloid jet

When an electric field (~10^5 V/m) is applied to a pendant droplet, the droplet

deforms into a conical shape, with a filament emanation from the apex. This phenomenon is referred to as the cone-jet transition, which denotes the form taken by the liquid meniscus at the point of ejection in the electric field.

Experiments in electrospray show the existence of and operating envelope within which the stability of the jet is maintained. At larger electric field strengths, skewed or multiple jets at the nozzle rim are observed. Outside the operating envelope the cone-jet transition is unstable. The pendant droplet first ejects a small droplet or long filament, and the liquid meniscus relaxes back to its initial position. In some studies, the unsteady emissions are referred to as cone-jet transitions. However, in this work the term ‘cone-jet transition’ refers only to the steady ejection of a liquid filament from a symmetric one. For other varieties and functioning modes of cone-jet transition, refer to the review articles by Cloupeau et al.

Nanocolloid jet is same the cone-jet term. A Colloid is a type of heterogeneous mixture. A colloid consists of two separate phases: a dispersed phase and a continuous phase. In a colloid, the dispersed phase is made of tiny particles of droplets that are distributed evenly throughout the continuous phase. The size of the dispersed phase particles are between 1nm and 1000nm in at least one dimension. So we called by the name of nanocolloid jet instead of cone-jet.

2.3 Pin-Pin type EHD nanocolloid jet printing system

The droplet size generated through cone-jet mode of electrohydrodynamic spraying ranges from 5nm up to 100μm, and its narrow distribution (geometrical standard deviation ~ 1.1) is one of the biggest advantages of electrohydrodynamic spraying.

Lee (2006) investigated the effect of the electrode diameter and the flow rate on

the pattern width by printed electrohydrodynamic printing. Yu (2006) examined the effect of electrode diameter and the flow rate on the pattern printed at the onset voltage where the cone-jet mode of electrohydrodynamic spraying. Conductive line patterning by electrohydrodynamic printing was firstly attempted by Lee et al. (2005). They used a toluene based silver nanoparticles suspension (30 wt%) made by ULVAC to form a conductive 1-D pattern that was first deposited onto a Kapton polyimide film, including a guide ring and pin (nozzle)-to-pin (ground) electrodes. Lee et al. (2006) used a ethylene glycol based silver nanoparticles suspension (20 wt%) made by Cabot and obtained a conductive line having 13 μΩ•cm resistivity that was about 8 folds higher than bulk silver(1.6 μΩ•cm). And they (2006) had two-dimensional patterning of conductive spiral-type that printed inductor measured 9.5 μΩ•cm and which shown figure 2-4 patterned various type.

The electrohydrodynamic printing system used in this study consisted of a nozzle, electrodes, power supply, and X-Y stage, as shown in Figure 2-3. A stainless steel nozzle (inner diameter: 180 μm, outer diameter: 320 μm) was used to produce a jet containing silver nanoparticles, which were uniformly supplied to the nozzle by a syringe pump (kds-100, KD Scientific Inc.) The nozzle was also used as anodes as well as a guide ring (inner diameter: 3.2 mm, outer diameter: 5.2 mm), which was located 0.03 mm below the nozzle. A pin-type electrode (400 nm in diameter) located 3.8 mm below the nozzle was used as the ground electrode to focus the jet onto the substrate, which was located 1.08 mm below the guide ring.

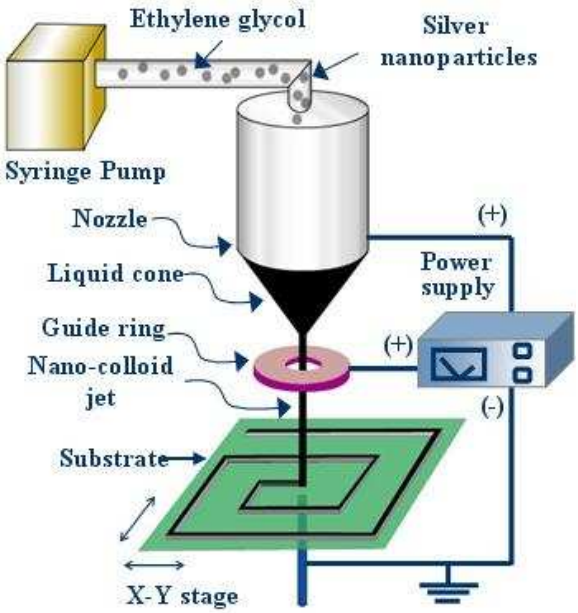

Figure 2-3 Schematic of Pin-Pin type printing system

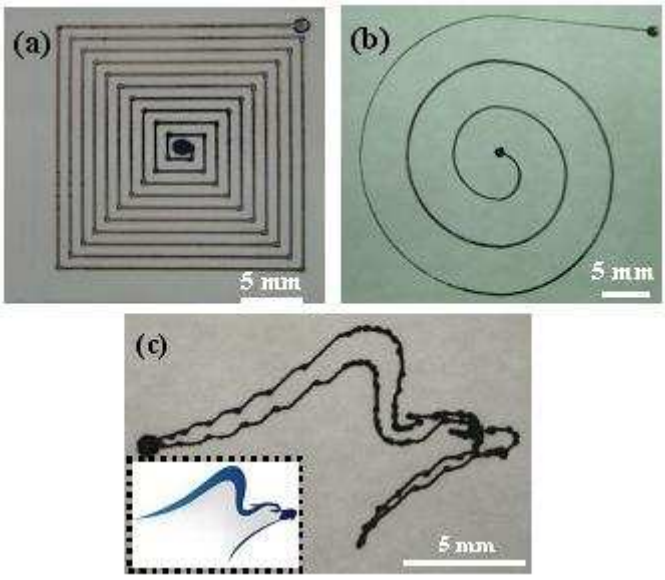

Figure 2-4 Square-shape pattern (a) round-shape (b) and one of the logos of Yonsei University (c) formed by electrohydrodynamic printing of silver nanoparticles

2.4 Problems of Pin-Pin type EHD nanocolloid jet printing system

When we experimented to gain patterns by using the Pin (nozzle)-to-Pin (ground) including a guide ring, we have to find some problems.

(1) The presence of a ground-pin electrode causes difficult alignment between nozzle and ground-pin. Because ground pin located under the substrate, we didn't able to perfectly alignment of centerline from nozzle to ground pin. When we have to set the nozzle and ground pin in the Pin-Pin type system, we depended on the manual method by using the eye. If this system misaligns a tiny, they will be able great to have an effect on pattern size.

(2) Printing dependent on the thickness and quality of substrate. Now, we had to use the substrate is photo paper and polyimide film in Pin-Pin type electrohydrodynamic nanocolloid jet printing. We used these materials because of ground pin under the substrate. When we used substrate of conductive material, ground pin is incapable to function.

(3) Available working distance of jetting is very narrow region. This system surely needed a regular space to below between substrate and ground pin

So we needed new concept of electrohydrodynamic printing system, which requires no ground-pin under the substrate and more easy setting of fixed alignment from nozzle to substrate.

3. Feasibility test of Pin-Lens type EHD system

3.1 Idea of Pin-Lens type system

We know that need the new concept of electrohydrodynamic printing system without ground pin under the substrate. Poon (2002) provided a idea of perfecting the printhead design. A special nozzle-ring configuration id devised to improve the deployment accuracy and makes the printing independent of the electrical and geometrical properties of substrate (Figure 3-1(a)) The jet is allowed to pass though the center of ring and impinge on the substrate. The idea originates from Melcher and Warren's experiments where they used a cylindrical wall electrode to establish a steady flow of a millimeter-sized glycerol filament. This configuration has an advantage that the formation of the cone-jet transition is purely determined by the applied potential difference between the nozzle and the first ring. Therefore, it eliminates the interference from surface irregularities on the substrate. In addition, the ring also serves as an electrostatic focusing device, which helps keep the jet staying along the centerline (Figure 3-1(b)). Figure 3-3(c) depicts the electric field between the ring and the bottom electrode.

Deitzel (2001) studied that electrospinning is a process by which sub-micron polymer fibers can be produced using and electrostatically driven jet of polymer solution(or polymer melt). It should be possible to design and electrospinning apparatus that can dampen or eliminate the bending instability through control of the shape and strength of the macroscopic electric field that exists as a result of the potential difference between the point of jet initiation and the collection target.(Figure 3-2(a) and (b))

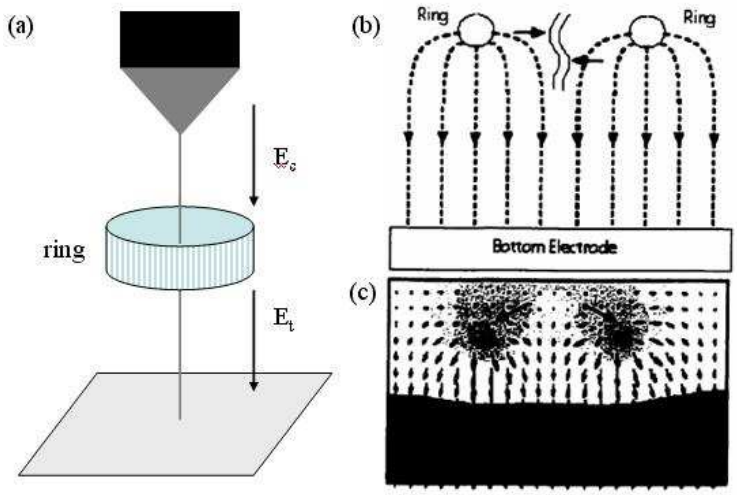

Figure 3-1 Idea of printhead design. (a)Schematic of nozzle-ring configuration to improve deployment accuracy and eliminate interferences from surface irregularities; (b) The converging electric field near the center axis of the ring tends to counteract with sinuous displacement for a positively charged jet. (c) The numerical simulation of electric field lines for the ring-plate configuration.

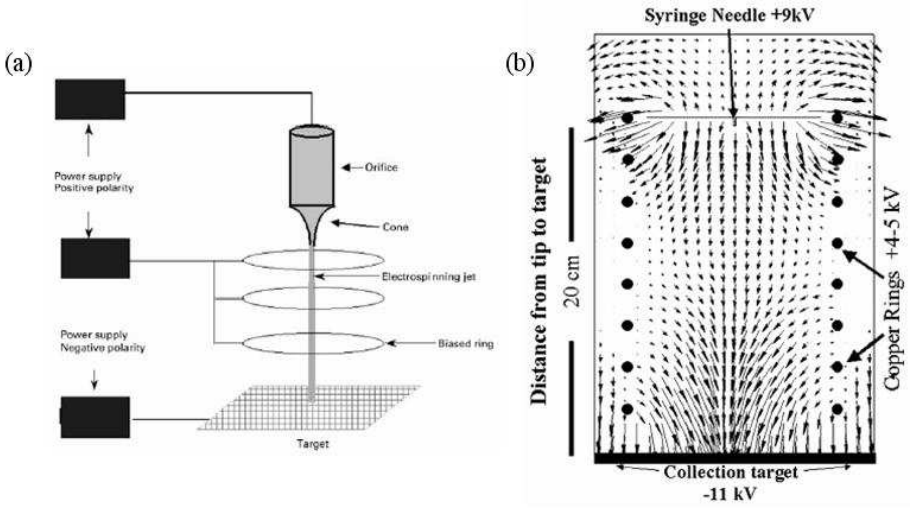

Figure 3-2 Multiple field electrospinning. (a) apparatus, (b) Fine lines calculated for multiple field electrospinning geometry

3.2 Experimental setting

The experimental setup consisted of a liquid supply system, an electrical system, and a moving stage system. The liquid supply system included a syringe pump (minimum flow rate: 16.7 pl/min for 1ml syringe) and a stainless steel nozzle (inner diameter: 180 μm, outer diameter: 360 μm). A silver nanoparticles suspension was injected downward from the nozzle. The moving stage system consisted of an X-Y moving stage and a digital control system, in which a programmable motion-controller that communicated directly with a PC controlled the motion of a substrate. The electrical system consisted of a high voltage power supply (~DC 15kV) and two electrodes. The nozzle used for the liquid supply system was also used as an anode as well as an electrohydrodynamic lens, which was located 2.0 mm below the nozzle (Figure 3-3). Figure 3-4 shows a magnified image of rectangular in Figure 3-3.

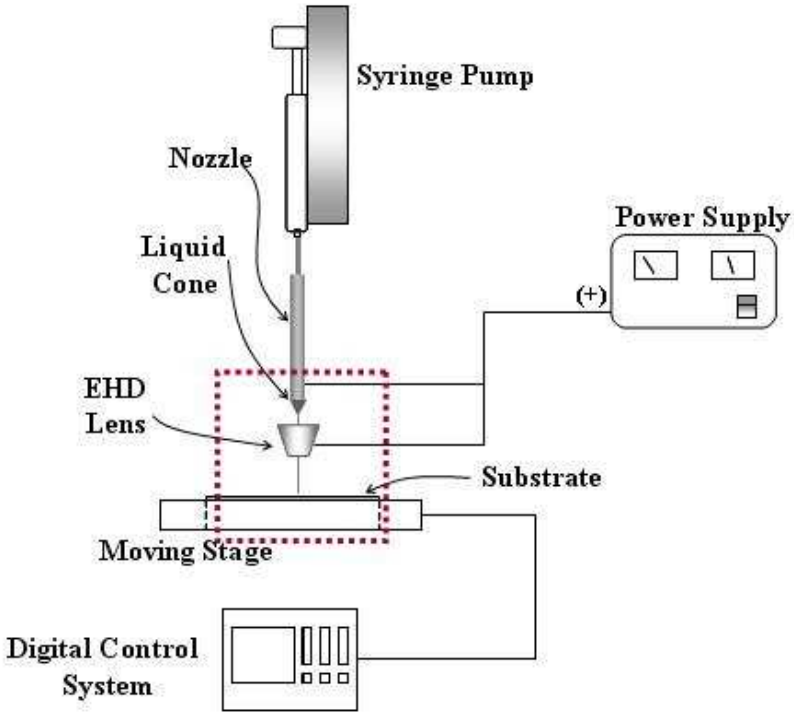

Figure 3-3 Schematic diagram of experimental setup

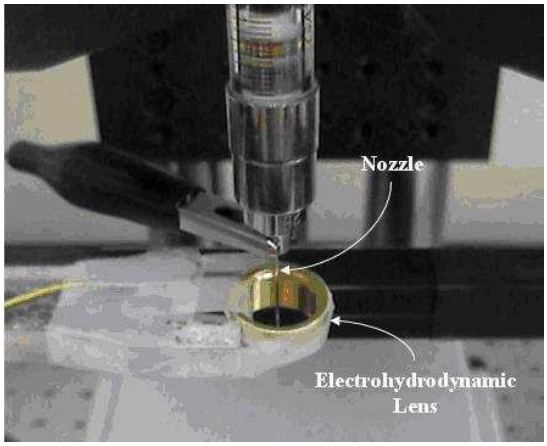

Figure 3-4 Magnified image of rectangular

3.3 Results

Experiments were carried out when the Type I lens was used. Type I lens has a cylinder-type inner hole and outer wall. Table 3-1 shows parameter of Type I lens. Figure 3-5 shows Type I lens. Even though the pin-type ground electrode was not used, patterns of silver nanoparticles were successfully obtained onto the substrate. Table 3-2 shows experimental conditions. Figure 3-6 shows that the pattern width by using the Type I lens was about 150 μm. Type I lens material is aluminum.

Figure 3-5 Type I lens

Table 3-1 Geometric of electrohydrodynamic lens (unit : mm)

EHD* lens	**Upper part**		**Lower part**		**Height**
	Outer	Inner	Outer	Inner	
Type I	10	6	10	6	6

* electrohydrodynamic

Table 3-2 Experimental Conditions & Pattern width

Test	**Case 1**	**Case 2**	**Case 3**
Voltage	6.5 kV	5.5 kV	5.0 kV
Flow rate	1 μl/min		
Pattern width	about 150 μm	about 130 μm	about 100 μm

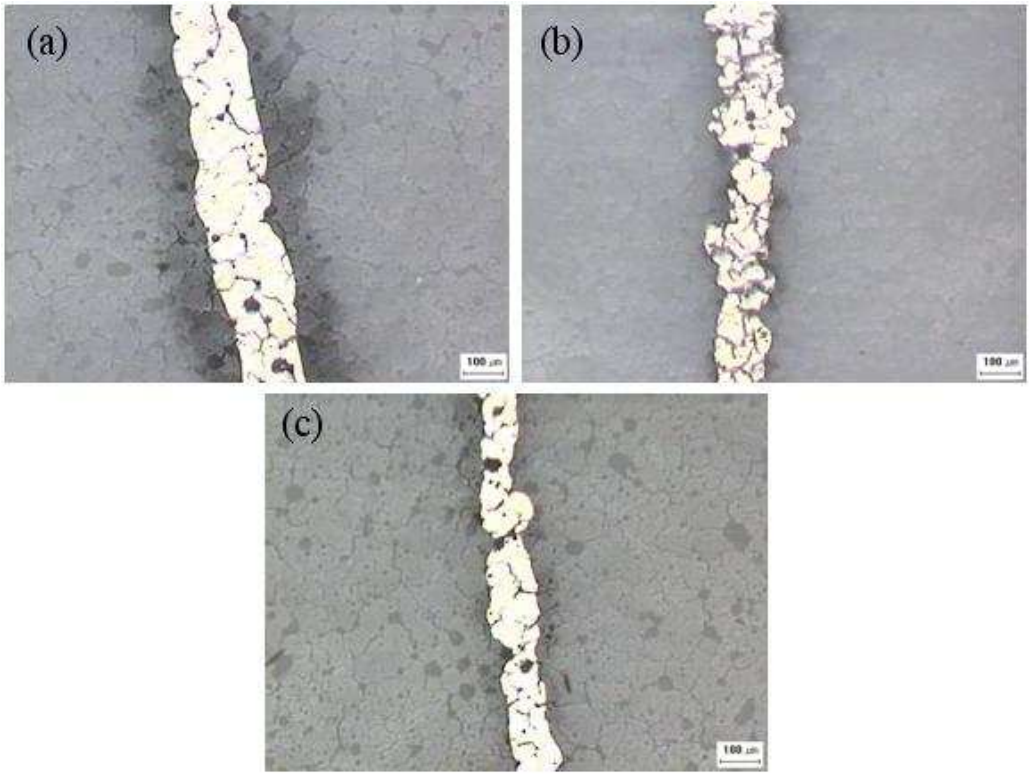

Figure 3-6 Patterned image by Type I lens; (a) case 1, (b) case 2, (c) case 3

Figure 3-7 is captured picture of electrohydrodynamic nanocolloid jet by high-speed camera at Pin-Pin type system. Each picture's interval is 0.04sec. As known to picture, EHD printing system need pulsed jet of several times for stable nanocolloid jet.

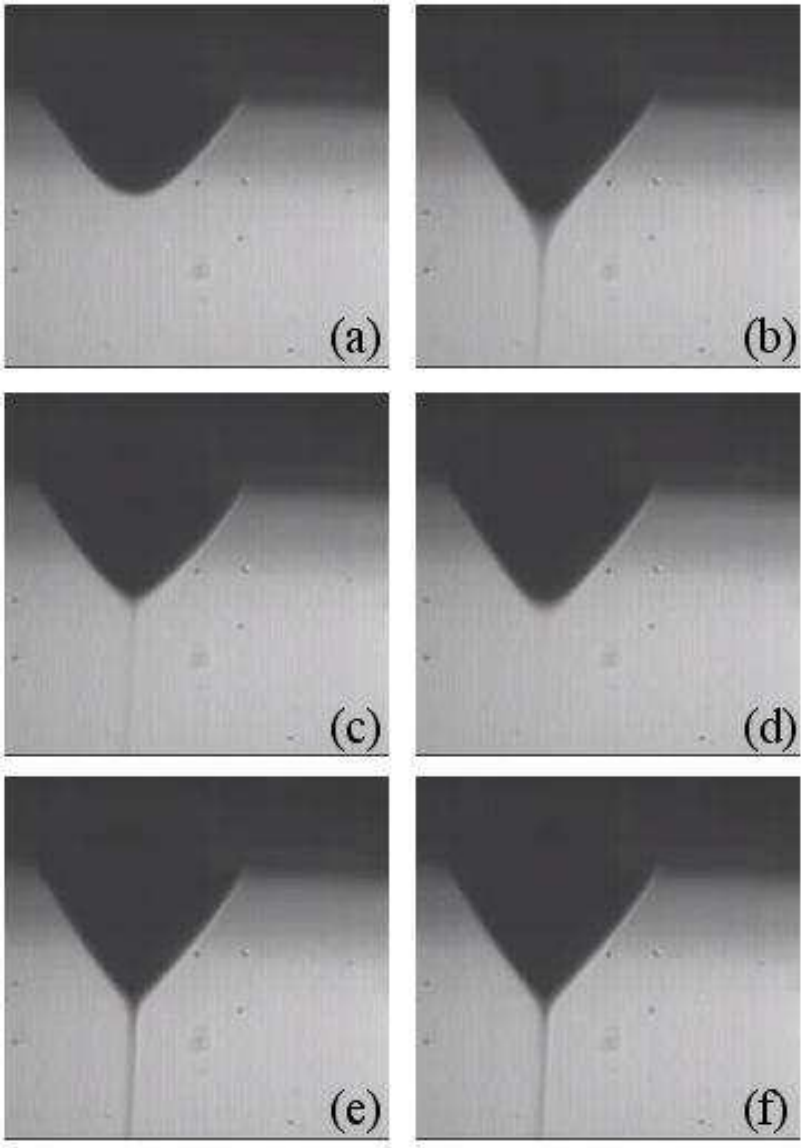

Figure 3-7 Captured picture of EHD nanocolloid jet

3.4 Objectives

This result is remarkable; however it's not satisfactory for obtaining more the fine patterns. So objective of my research sets up the three boundaries. First of all is to easy setting the experiment, second is focusing for gain the fine pattern and third is to improve stabilizing in substrate of various materials.

(1) Easy set up the alignment

Pin-Lens type experiment easily set up the alignment between nozzle and ground how to design of electrohydrodynamic lens. The answer is mix up the guide ring and ground electrode.

(2) Focusing

Secondly important object is focusing. Experiment of Pin-Lens type need to gain more fine patterns than Pin-Pin type.

(3) Stabilizing

Third important object is that we will be to gain the stabilizing electro-hydrodynamic nanocolloid jet How to design of electrohydrodynamic lens, through a modified geometry of lens.

So this thesis tries that various geometry of electrohydrodynamic lens analysis by using the commercial solver package. And we compare pattern result with physical modeling result.

4. Physical modeling of EHD lens for focusing and stabilizing

4.1 Introduction

Maxwell 3D (version 10)

Maxwell is a high-performance interactive software package that uses finite element analysis (FEA) to solve tree-dimensional (3D) electric, magnetostatic, eddy current, and transient problems. This program uses it to compute that static electric field, forces, torques, and capacitances caused by voltage distributions and charges, static magnetic fields, forces torque, and inductances caused by DC currents, static external magnetic fields, and permanent magnets, time-varying magnetic fields, forces, torques, and impedances caused by AC currents and oscillation external magnetic fields, and transient magnetic fields caused by electrical sources and permanent magnets.

COMSOL Multiphysics (3.2b)

COMSOL Multiphysics is a modeling package for the simulation of any physical process you can describe with partial differential equations (PDEs). It features state-of-the-art solvers that address complex problems quickly and accurately, while its intuitive structure is designed to provide ease of use and flexibility. We can easily model most phenomena through predefined modeling templates. Modifying these to specific applications is possible through equation-based modeling capabilities. To deal with the increasing demand for realistic representations of the world around us, we can easily model systems of coupled physics phenomena. COMSOL Multiphysics provides

a friendly, fast and versatile environment for multiphysics modeling. Fast results and unprecedented flexibility make COMSOL Multiphysics the ideal modeling and simulation software for research, product development, and education.

This thesis was to use both Maxwell and COMSOL Multiphysics for Physical modeling of electrohydrodynamic lenses.

4.2 Design of electrohydrodynamic lens

When I was to use Type I lens, its geometry is cylinder-type, and try various geometry of lens. Figure 4-1 shows drawing four types lens by using Maxwell package. Type I lens has a cylinder-type inner hole and outer wall while Type II lens has a cone-type inner hole and cylinder-type outer wall. Type III lens has a cone-type inner hole and outer wall and Type IV lens also has the same type as Type III lens but the thinner thickness than that of the Type III lens. The detail geometries of electrohydrodynamic lenses of four types are summarized at Table 4-1.

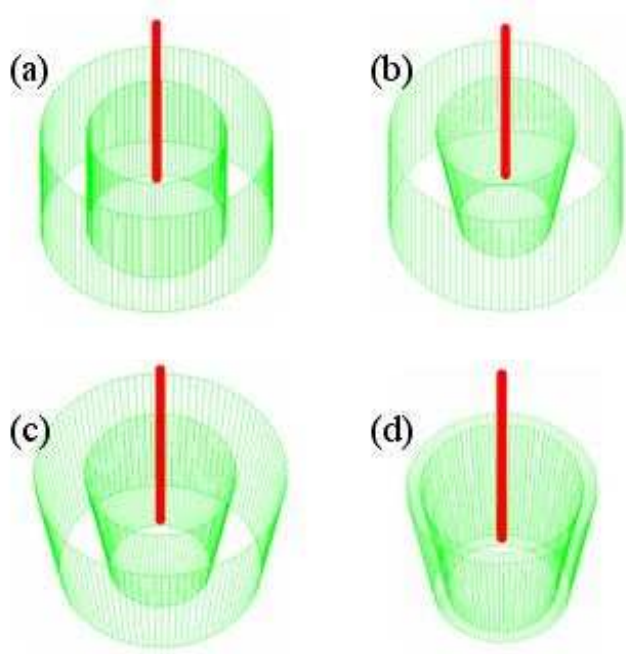

Figure 4-1 Design of electrohydrodynamic lens;

(a) Type I, (b) Type II, (c) Type III, (d) Type IV

Table 4-1 Geometric of electrohydrodynamic lens (unit : mm)

EHD* lens	Upper part		Lower part		Height
	Outer	Inner	Outer	Inner	
Type I	10	6	10	6	6
Type II	10	6	10	4	6
Type III	10	6	8	4	6
Type IV	7	6	5	4	6

* Electrohydrodynamic

4.3 Simulation results

Numerical calculations were carried out to predict the effects of the electrohydrodynamic lens on electric field strengths. One of the principal cornerstones of electrostatics is the posing and solving of problems that are described by the Poisson equation. Finding φ for some given *f* is an important practical problem, since this is the usual way to find the electric potential for a given charge distribution. In SI units:

$$\nabla^2 \Phi = -\frac{\rho}{\epsilon_0}$$

where Φ is the electric potential (in volts), ρ is the charge density (in coulombs per cubic meter), and ϵ_0 is the permittivity of free space (in farads per meter).

In a region of space where there is no unpaired charge density, we have

$$\rho = 0,$$

and the equation for the potential becomes Laplace's equation:

$$\nabla^2 \Phi = 0.$$

Figure 4-2 shows two dimensional electric field strengths of four types of lens between the nozzle and the lens. As shown in Figure 4-3, the dotted lines in picture indicated the degree of dispersion of electric field strength. When the Type IV lens was used, the electric field strength was concentrated near the center of the lens and thus narrow electric fields were generated at the end of the lens. Consequently, it is expected that the jet break up would be minimized when Type IV lens used.

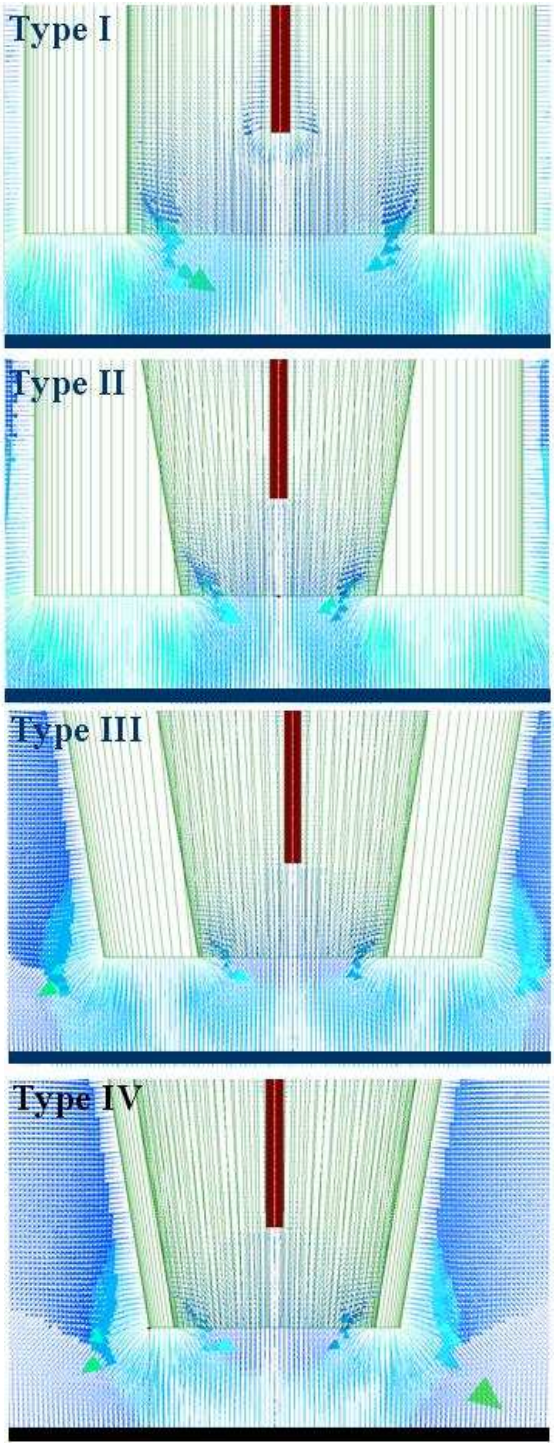

Figure 4-2 Maxwell analysis of electrohydrodynamic lens

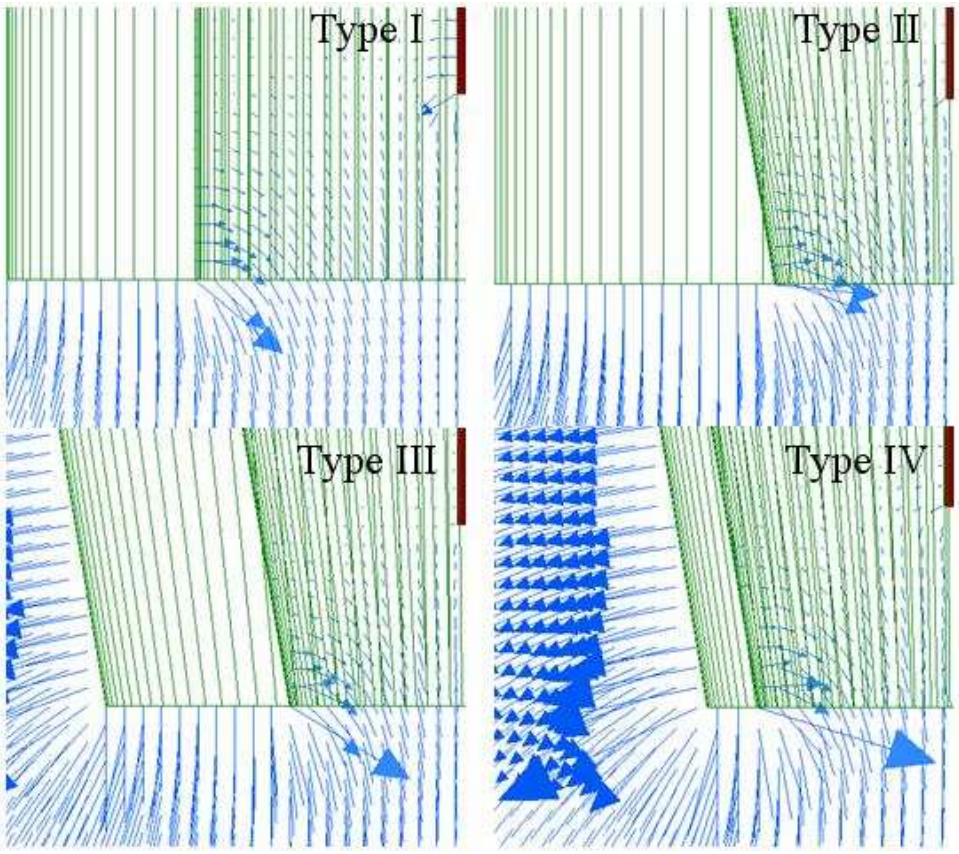

Figure 4-3 Maxwell analysis of electrohydrodynamic lens (corner parts of magnified)

Because Maxwell results can’t explain exactly about focusing, this physical modeling uses the COMSOL Multiphysics. This program proves about focusing at Nature Nanotechnology. From Figure 4-4 to Figure 4-8, which results are by using COMSOL Multiphysics. As previously stated, this program is very useful about drawing of electrical strength field.

Figure 4-4 shows overall result of physical modeling by COMSOL. These figure use contour line of 40 and stream line. A contour map is a map illustrated with contour lines, for example a topographic map. The prefix iso-, from the Greek prefix ισος ("equal"), is used from descriptive names for map lines that join points of equal value. Streamlines are a family of curves that are instantaneously tangent to the velocity vector of the flow. This means that if a point is picked then at that point the flow moves in a certain direction. Moving a small distance along this direction and then finding out where the flow now points would draw out a streamline. The results of Figure 4-5 is drawing contour lines of 40. To further confirmed with much circumstance of result, Figure 4-6 shows contour line of 20. Figure 4-7 shows contour line and stream line about simulation results of each lens. Synthetically, Type II lens of focusing effect is better than Type I lens. Actually, between Type II lens and Type IV lens can’t explain about improvement of focusing effect. However, we can explain to improve stabilization between Figure 4-6(b) and Figure 4-6(d), because Type IV lens shows more flat interval line than Type II lens.

Figure 4-8 shows between Type III lens and Type III-a lens about simulation result of contour line and stream line. Accordingly transformation of an external form, Figure 4-8 shows to improve effect of focusing. Because stream line gap of Type III-a lens is more narrow than Type III lens.

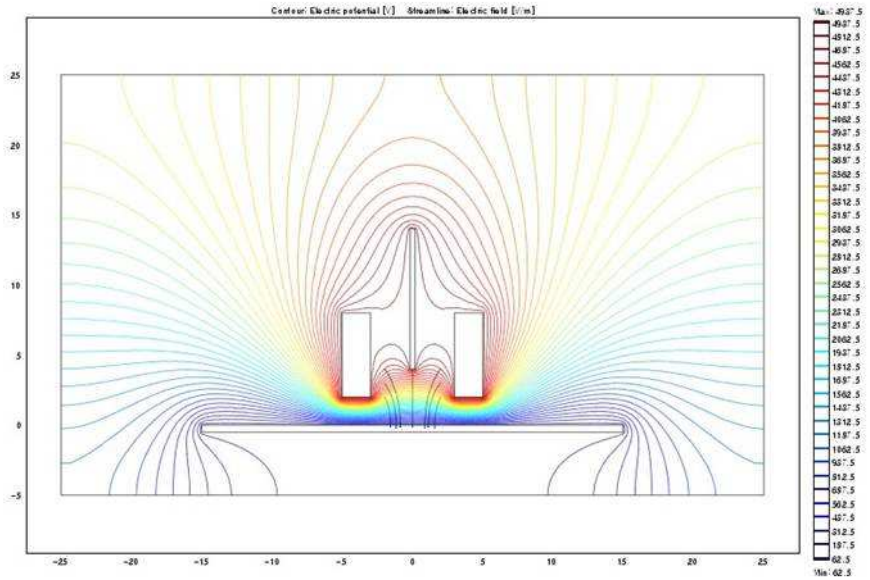

Figure 4-4(a) COMSOL analysis of electrohydrodynamic Type I lens (overall)

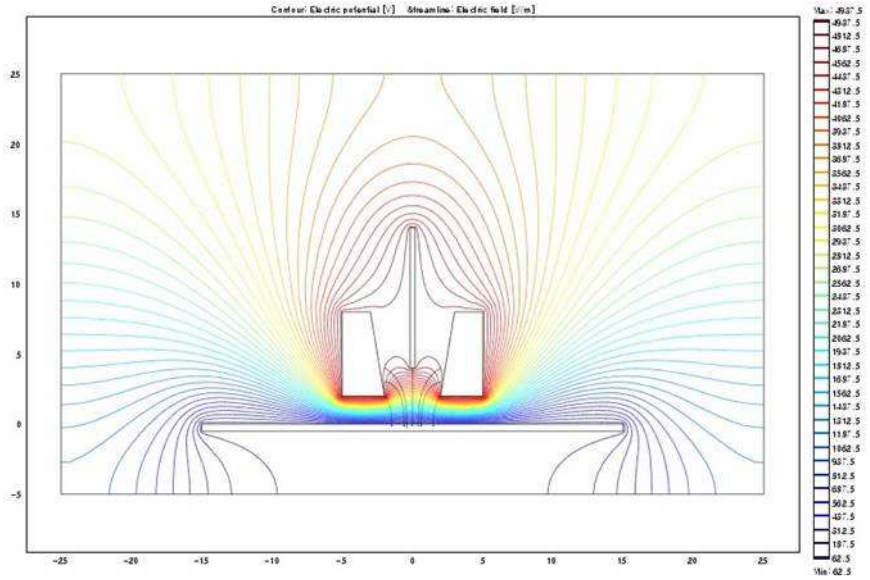

Figure 4-4(b) COMSOL analysis of electrohydrodynamic Type II lens (overall)

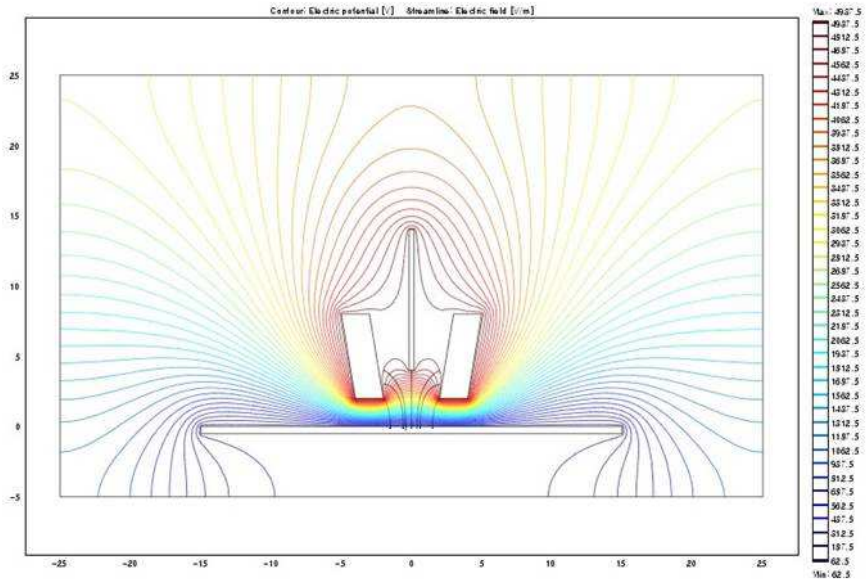

Figure 4-4(c) COMSOL analysis of electrohydrodynamic Type III lens (overall)

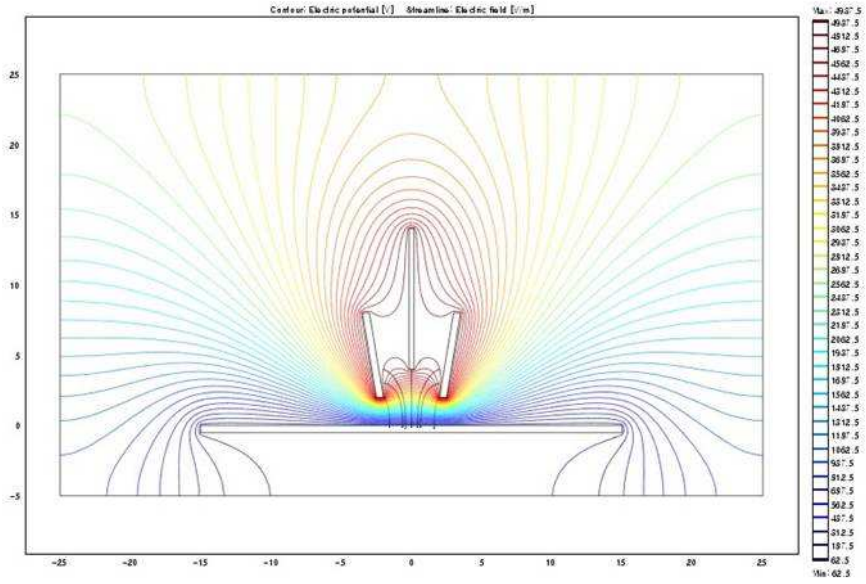

Figure 4-4(d) COMSOL analysis of electrohydrodynamic Type IV lens (overall)

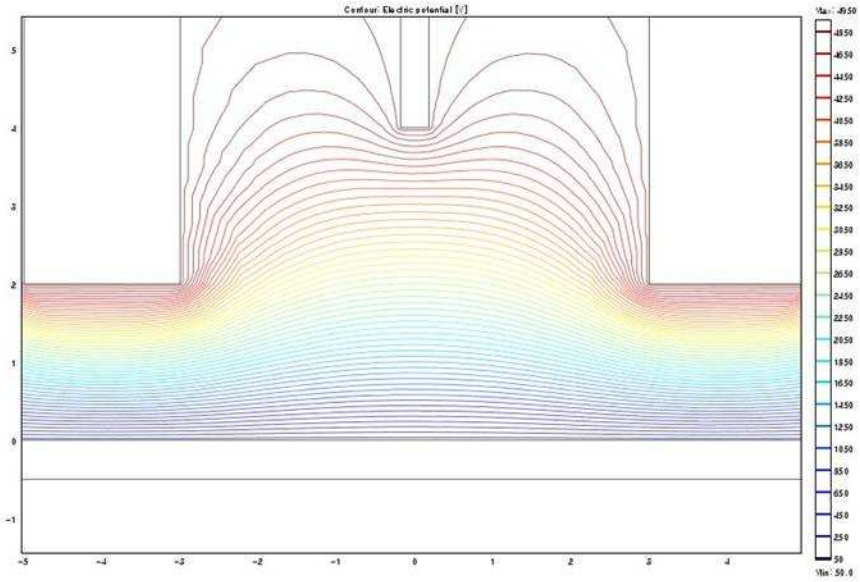

Figure 4-5(a) COMSOL analysis of electrohydrodynamic Type I lens (Contour 40)

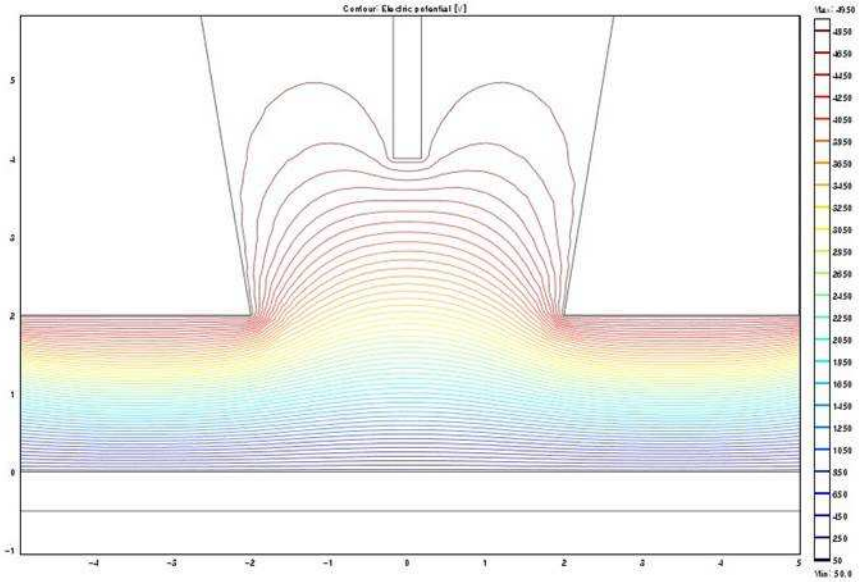

Figure 4-5(b) COMSOL analysis of electrohydrodynamic Type II lens (Contour 40)

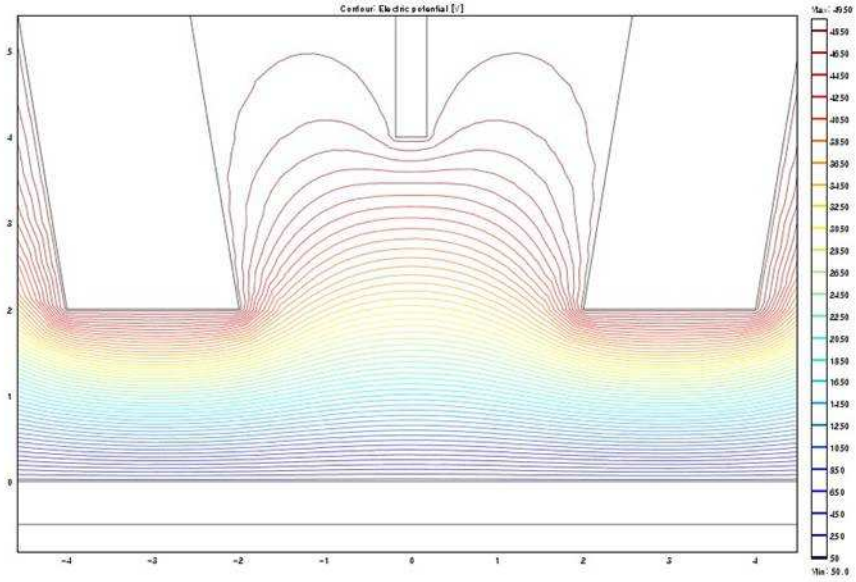

Figure 4-5(c) COMSOL analysis of electrohydrodynamic Type III lens (Contour 40)

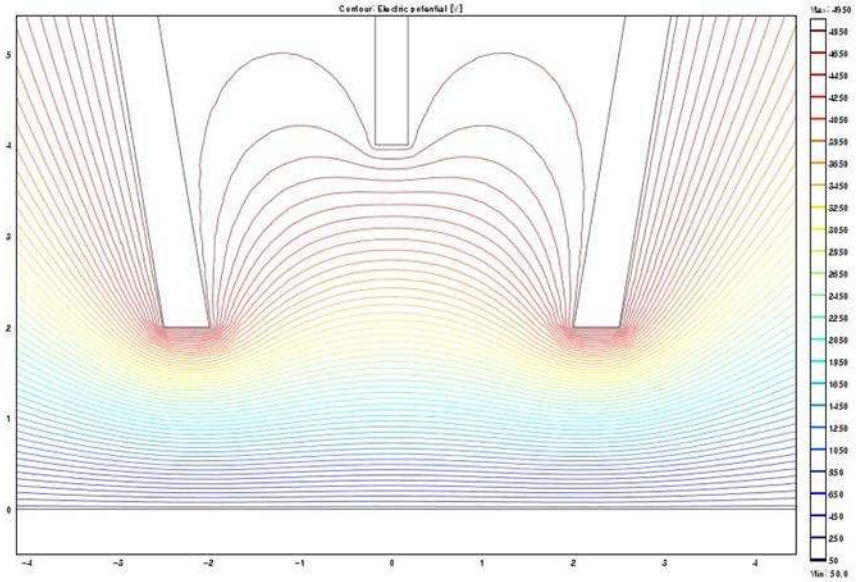

Figure 4-5(d) COMSOL analysis of electrohydrodynamic Type IV lens (Contour 40)

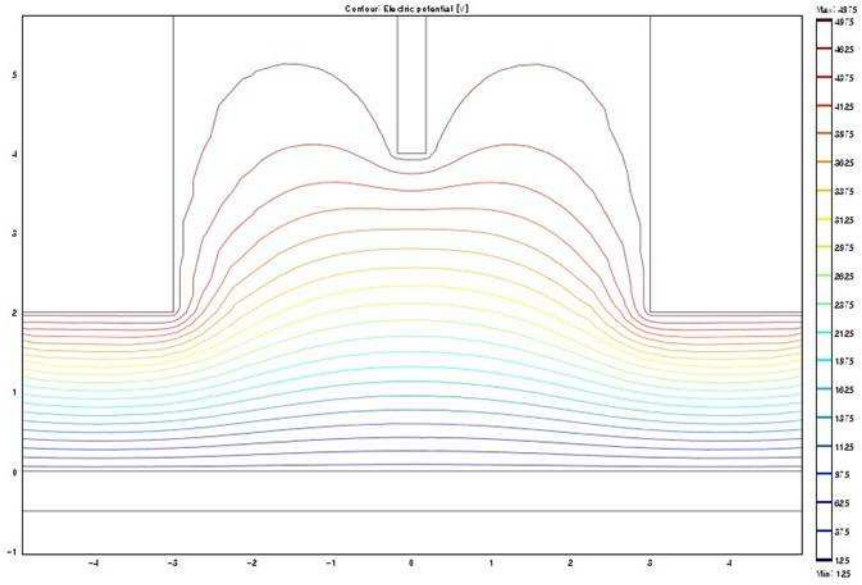

Figure 4-6(a) COMSOL analysis of electrohydrodynamic Type I lens (Contour 20)

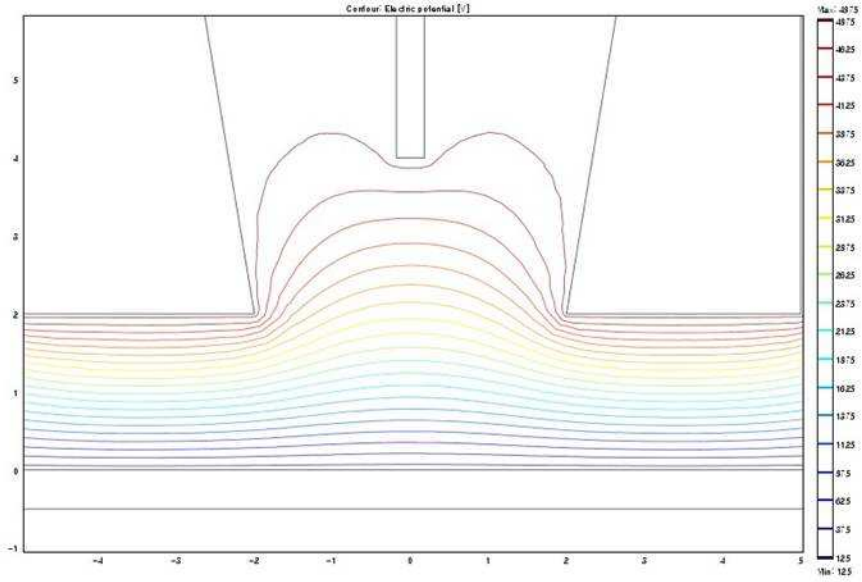

Figure 4-6(b) COMSOL analysis of electrohydrodynamic Type II lens (Contour 20)

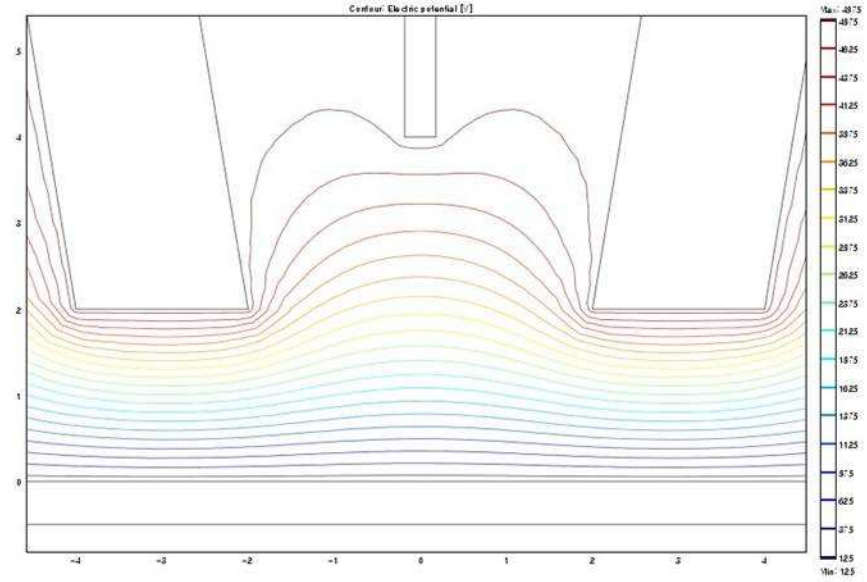

Figure 4-6(c) COMSOL analysis of electrohydrodynamic Type III lens (Contour 20)

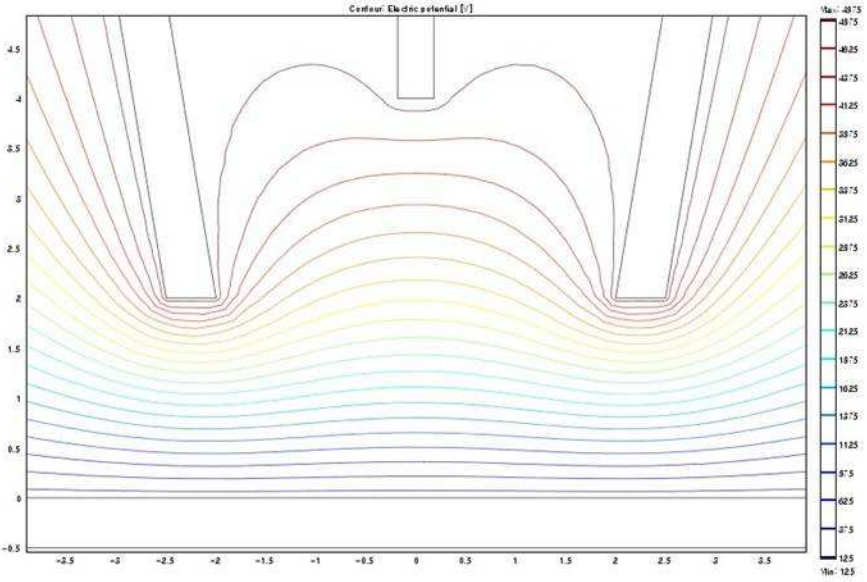

Figure 4-6(d) COMSOL analysis of electrohydrodynamic Type IV lens (Contour 20)

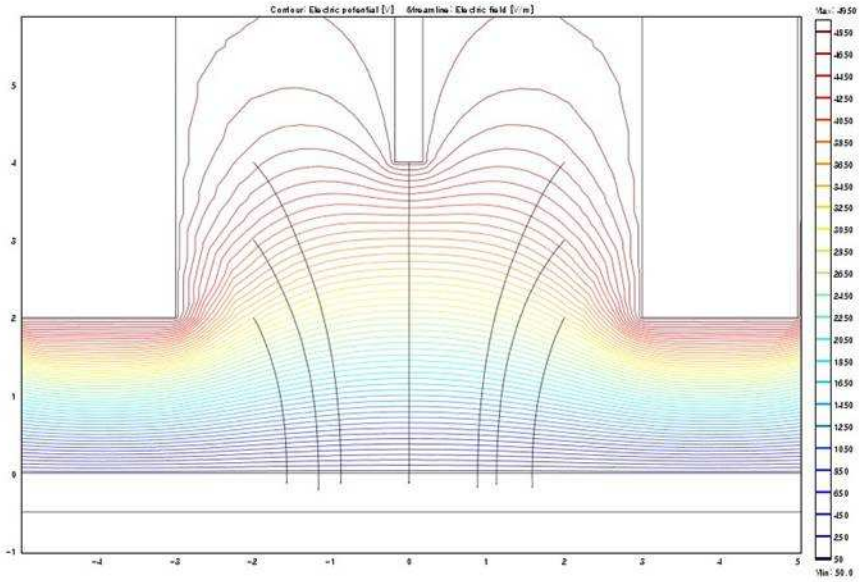

Figure 4-7(a) COMSOL analysis of electrohydrodynamic Type I lens (Contour 40 & Stream line)

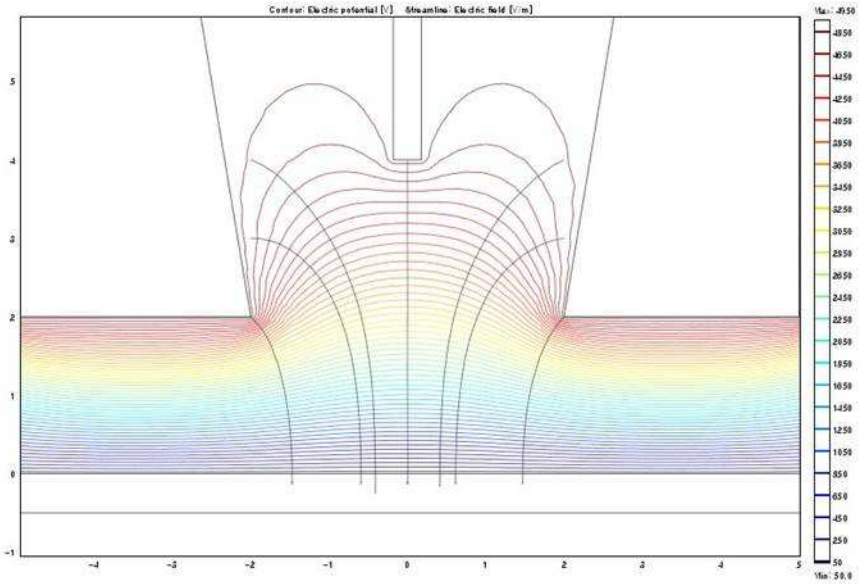

Figure 4-7(b) COMSOL analysis of electrohydrodynamic Type II lens (Contour 40 & Stream line)

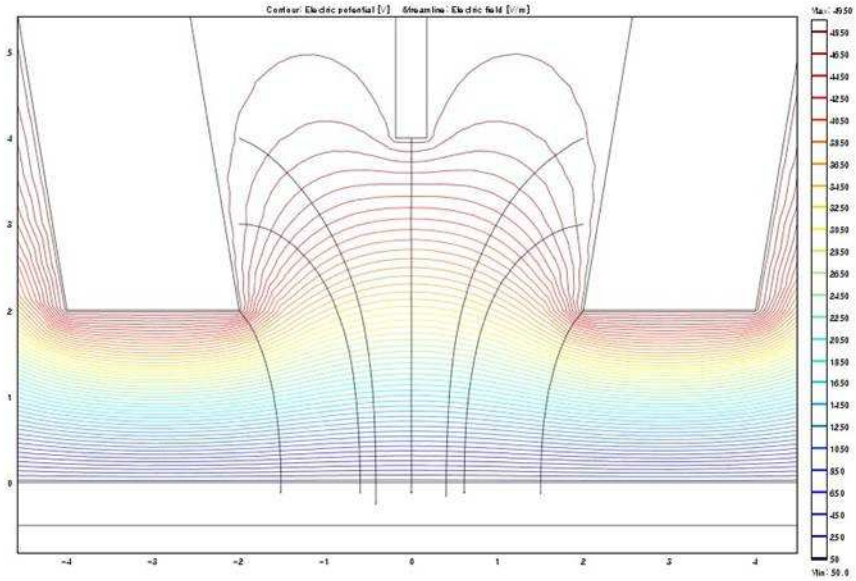

Figure 4-7(c) COMSOL analysis of electrohydrodynamic Type III lens (Contour 40 & Stream line)

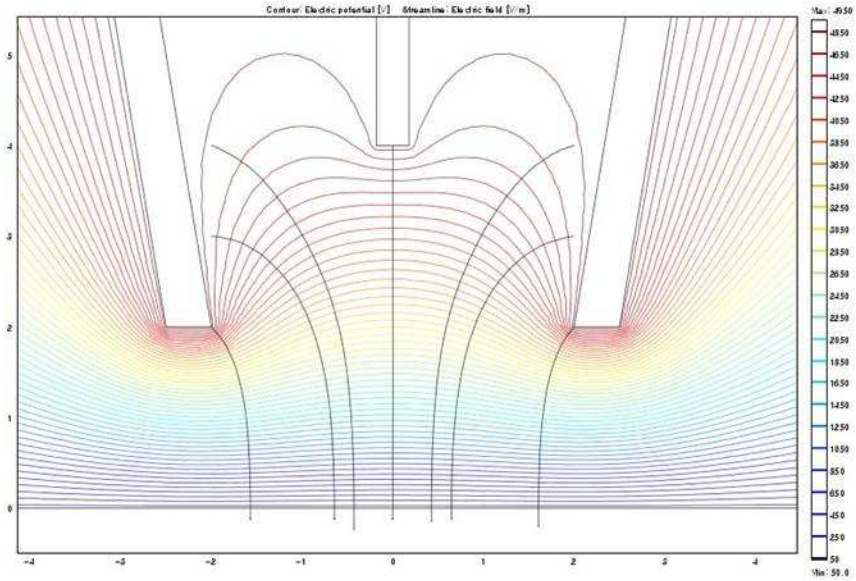

Figure 4-7(d) COMSOL analysis of electrohydrodynamic Type IV lens (Contour 40 & Stream line)

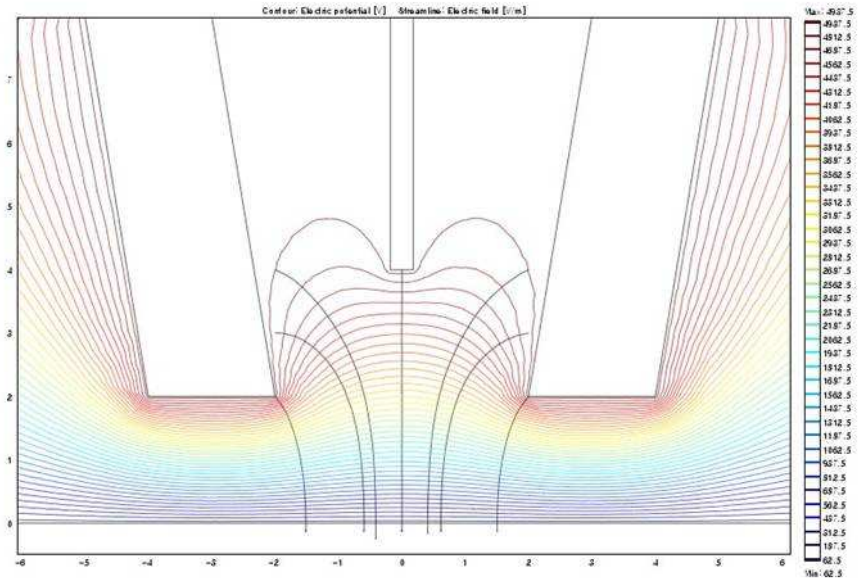

Figure 4-8(a) COMSOL analysis of electrohydrodynamic Type III lens (Contour 40 & Stream line)

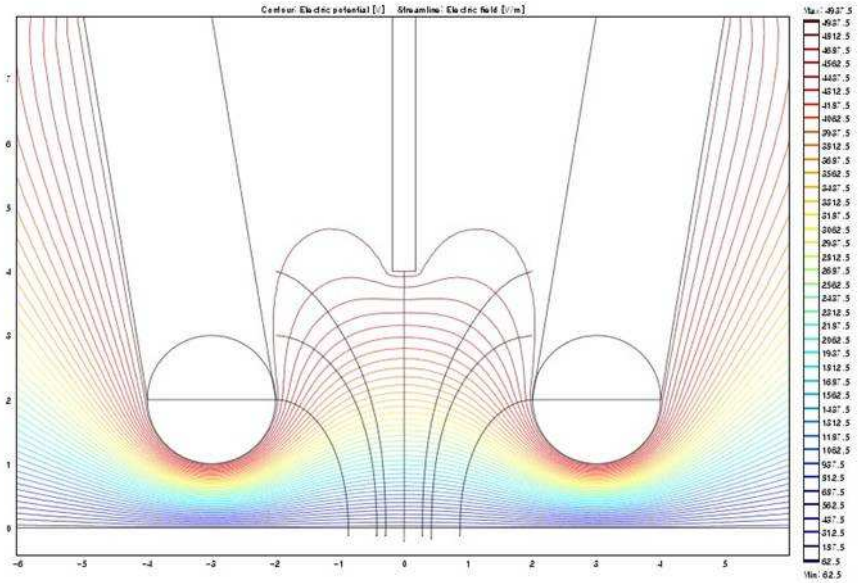

Figure 4-8(b) COMSOL analysis of electrohydrodynamic Type III-a lens (Contour 40 & Stream line)

4.4 Calculation results

Origin (version 7.0)

Origin is available in many different forms ranging from a single user package to an institution or company-wide site license. In multiple-copy licenses, Origin includes concurrent license management, allowing you to install the software on as many computers as you need. Origin can also be applied as an OEM (Original Equipment Manufacturer) solution for instrument manufacturers.

Figure 4-9 shows concept for gain the data. Figure 4-9(a) is filled out diagram and Figure 4-9(b) is frame diagram. From Line 1 to 3 locate 0.1, 1 and 1.9mm at substrate. Line 1 is just before the impingement at substrate, Line 3 is actually to generate location by cone-jet mode, and Line 2 is to locate middle between Lens and substrate. Figure 4-10 shows located line each Lens. Figure 4-11 show electric field strength at each line. These graphs explain by Coulomb's force. Coulomb's law is the mathematical consequence of law of conservation of linear momentum in exchange by virtual photons in 3-dimensional space (see quantum electrodynamics). Scalar form is interested only in the magnitude of the force, and not in its direction, it may be easiest to consider a simplified, scalar version of the law:

$$F = k_C \frac{|q_1||q_2|}{r^2}$$

where F is the magnitude of the force exerted, q_1 is the charge on one body, q_2 is the charge on the other body, r is the distance between them,

$k_C = \frac{1}{4\pi\epsilon_0} \approx$ 8.988×109 N m2 C-2 (also m F-1) is the electrostatic constant or Coulomb force constant, and $\epsilon_0 \approx$ 8.854×10^{-12} $C^2N^{-1}m^{-2}$ (also F m^{-1}) is the permittivity of free space, also called electric constant, an important physical constant.

This formula says that the magnitude of the force is directly proportional to the magnitude of the charges of each object and inversely proportional to the square of the distance between them. When measured in units that people commonly use (such as MKS - see International System of Units), the Coulomb force constant, k, is numerically much larger than the universal gravitational constant G. This means that for objects with charge that is of the order of a unit charge (C) and mass of the order of a unit mass (kg), the electrostatic forces will be so much larger than the gravitational forces that the latter force can be ignored. This is not the case when Planck units are used and both charge and mass are of the order of the unit charge and unit mass. However, charged elementary particles have mass that is far less than the Planck mass while their charge is about the Planck charge so that, again, gravitational forces can be ignored. The force F acts on the line connecting the two charged objects. Charged objects of the same polarity repel each other along this line and charged objects of opposite polarity attract each other along this line connecting them. Coulomb's law can also be interpreted in terms of atomic units with the force expressed in Hartrees per Bohr radius, the charge in terms of the elementary charge, and the distances in terms of the Bohr radius.

Electric field follows from the Lorentz Force Law that the magnitude of the electric field E created by a single point charge q is

$$|E| = \frac{1}{4\pi\epsilon_0}\frac{|q|}{r^2}$$

For a positive charge q, the direction of E points along lines directed radially away from the location of the point charge, while the direction is the opposite for a negative charge. Units: volts per meter or newtons per coulomb.

As previously explained, the more electric field strength is higher, the more repulsive force is higher. So, as show to seen Figure 4-11(c), because Type IV lens is to generate highest electric field strength, radial force of outside effect is very little.

Data of Each line gained by the Maxwell, as show likely between Figure 4-12 and Figure 4-15, which arrange by Origin as form of Matrix 3-dimension. Figure 4-12 show Z axial force fixed Z axial by X-Y at each lens. Type IV lens generate to effect of focus better than others. Figure 4-13 show as same condition Figure 4-12. Between Figure 4-14 and Figure 4-15 show Y axial fore fixed Y axial by X-Z at each lens. Because low rough of graph face is little effect of radial force, these graphs explain about stabilization.

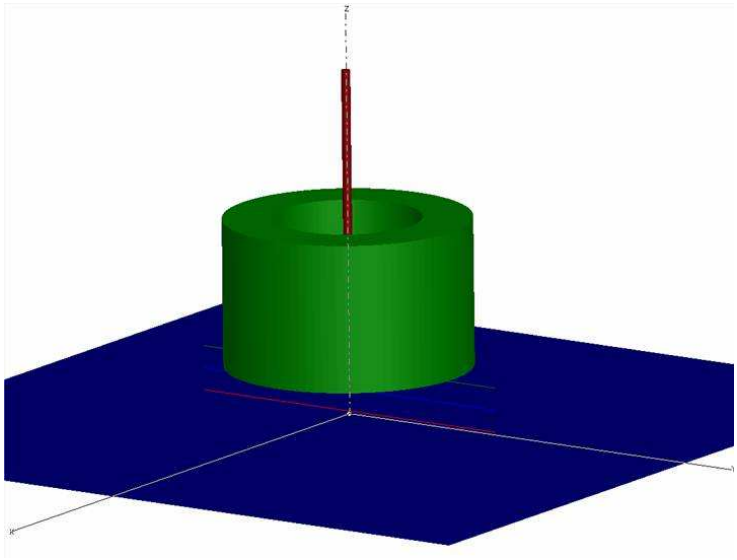

Figure 4-9(a) Diagram of Data line

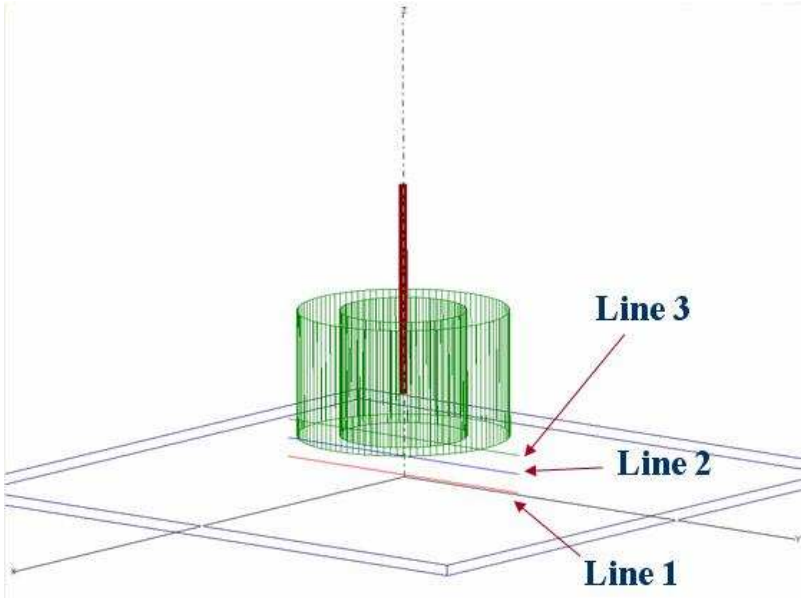

Figure 4-9(b) Diagram of Data line

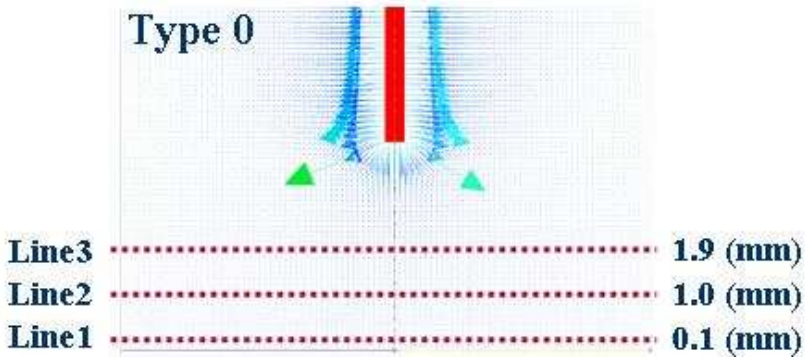

Figure 4-10(a) Diagram of Data line without lens

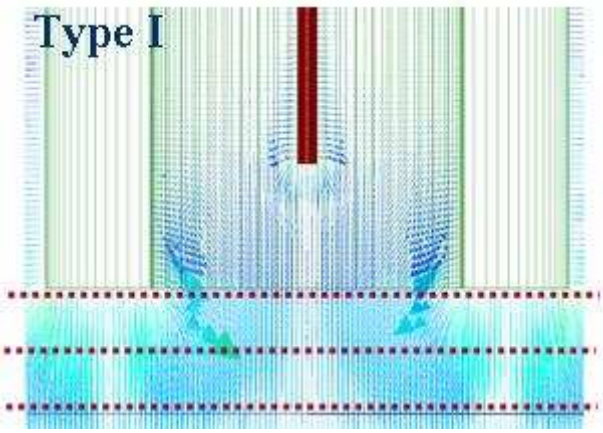

Figure 4-10(b) Diagram of Data line Type I lens

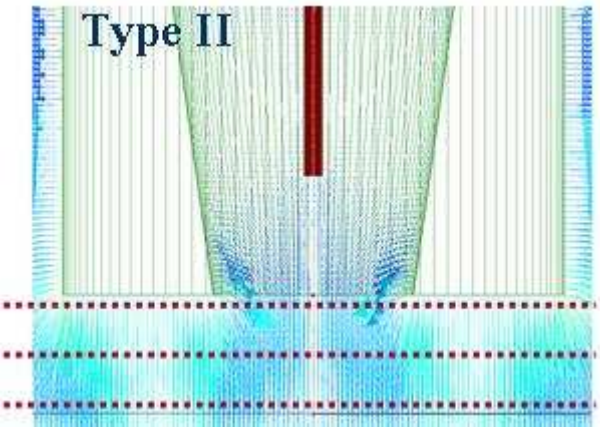

Figure 4-10(c) Diagram of Data line Type II lens

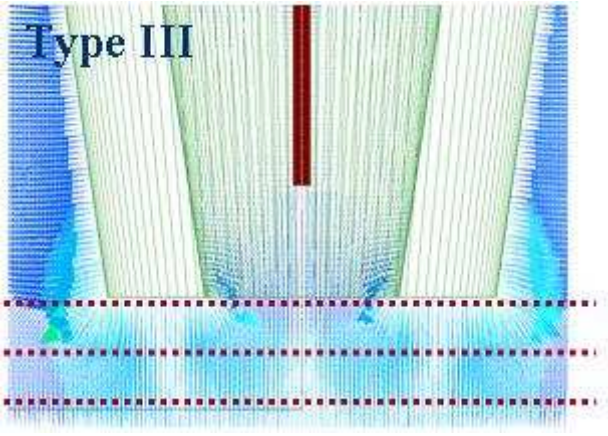

Figure 4-10(d) Diagram of Data line Type III lens

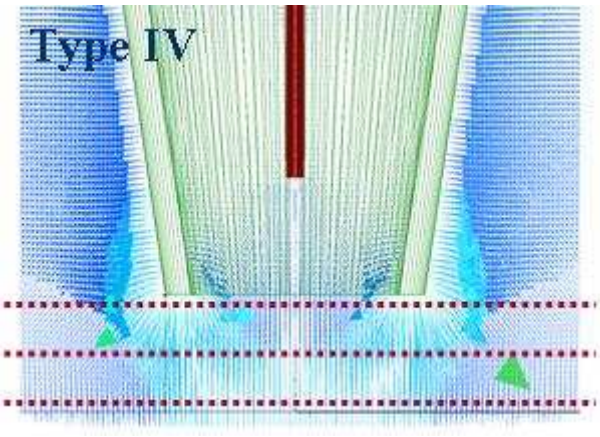

Figure 4-10(e) Diagram of Data line Type IV lens

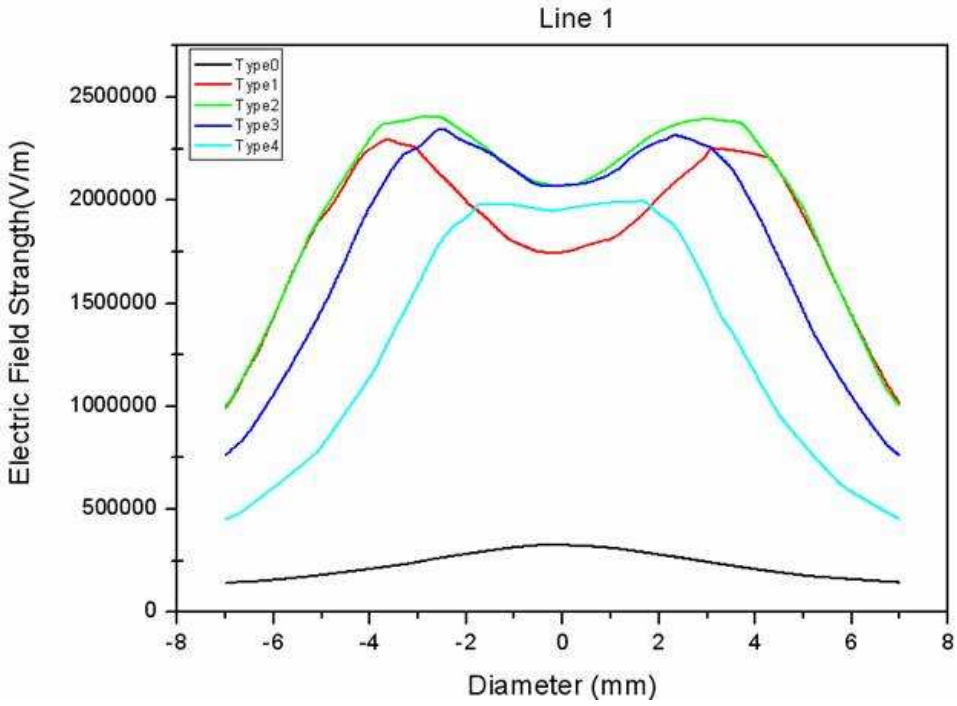

Figure 4-11(a) Graph of Line 1 (Upper 0.1mm at substrate)

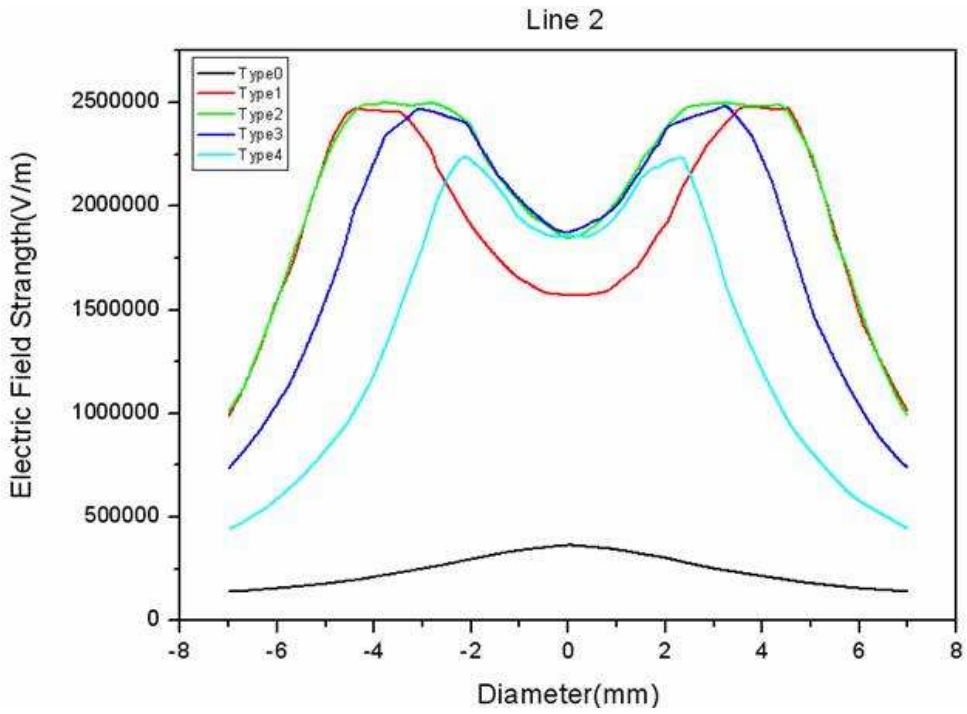

Figure 4-11(b) Graph of Line 2 (Upper 1.0mm at substrate)

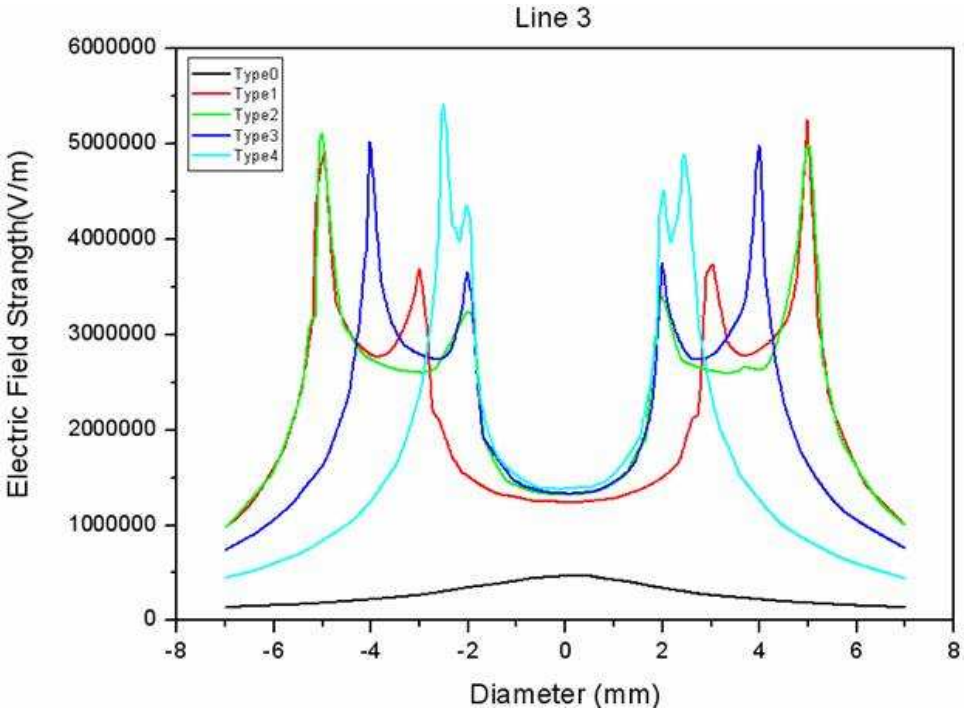

Figure 4-11(c) Graph of Line 3 (Upper 1.9mm at substrate)

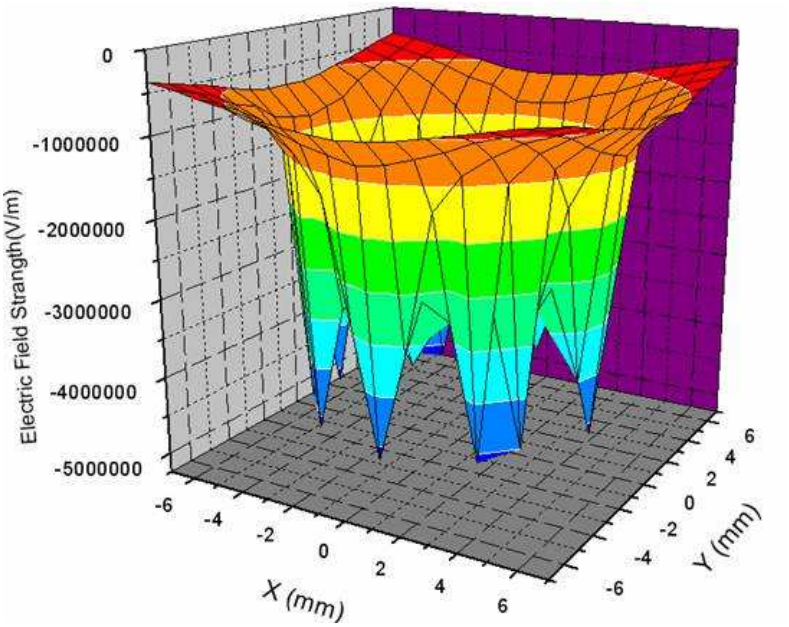

Figure 4-12(a) Matrix calculation of Type I lens at Line 3
(Fixed Z axial; 1.9mm to substrate)

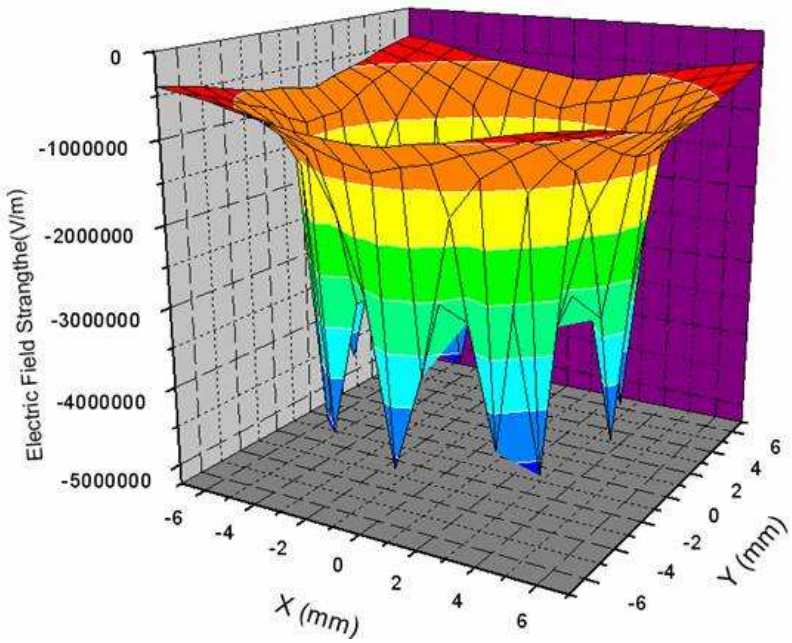

Figure 4-12(b) Matrix calculation of Type II lens at Line 3
(Fixed Z axial; 1.9mm to substrate)

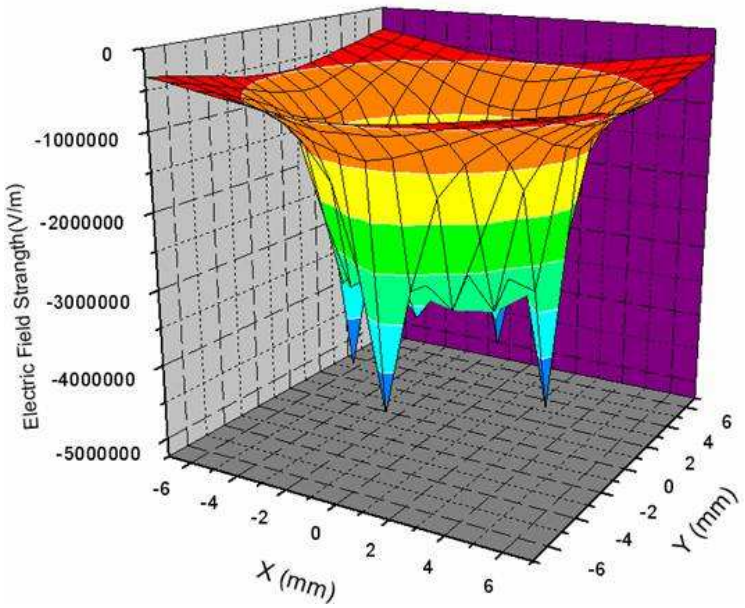

Figure 4-12(c) Matrix calculation of Type III lens at Line 3
(Fixed Z axial; 1.9mm to substrate)

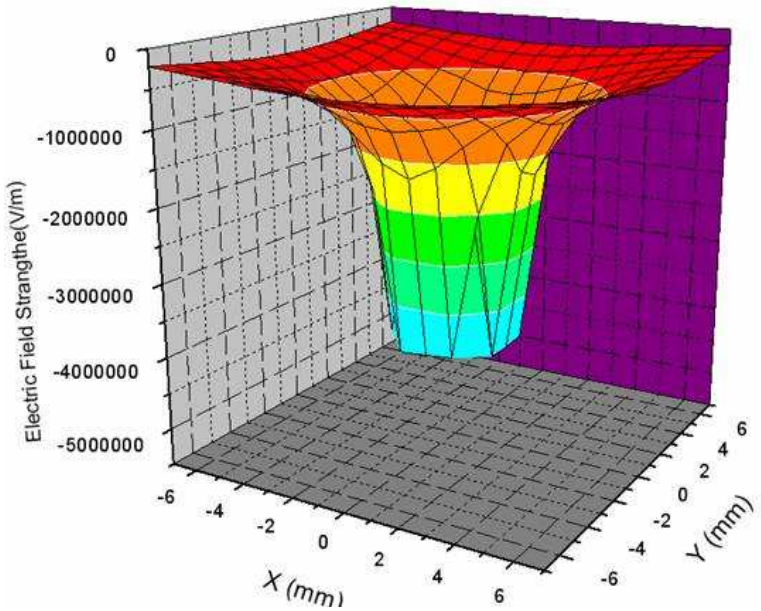

Figure 4-12(d) Matrix calculation of Type IV lens at Line 3
(Fixed Z axial; 1.9mm to substrate)

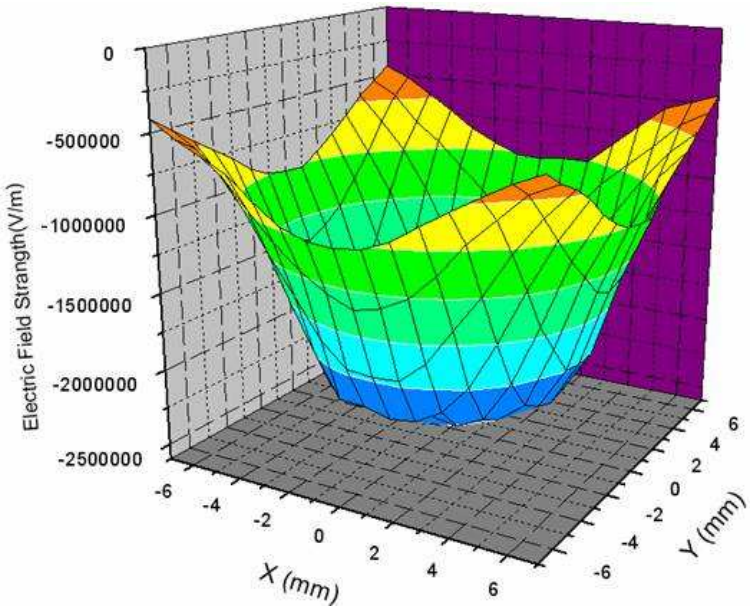

Figure 4-13(a) Matrix calculation of Type I lens at Line 1
(Fixed Z axial; 0.1mm to substrate)

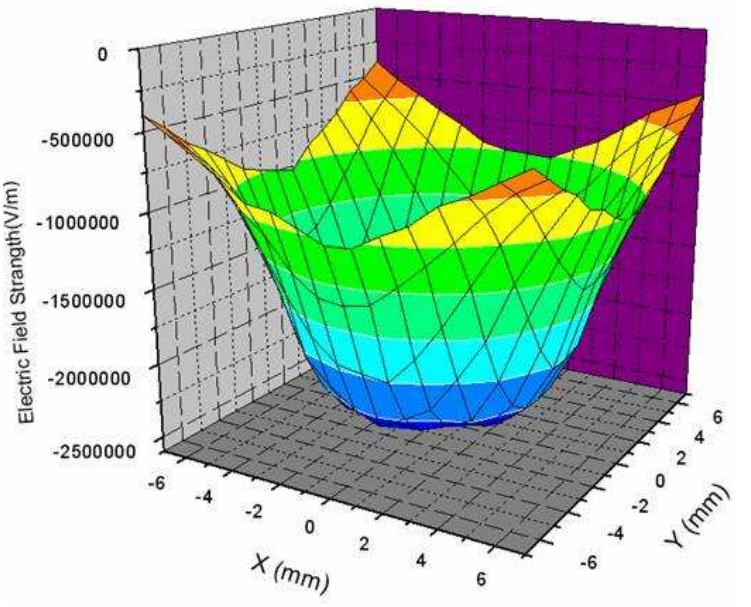

Figure 4-13(b) Matrix calculation of Type II lens at Line 1
(Fixed Z axial; 0.1mm to substrate)

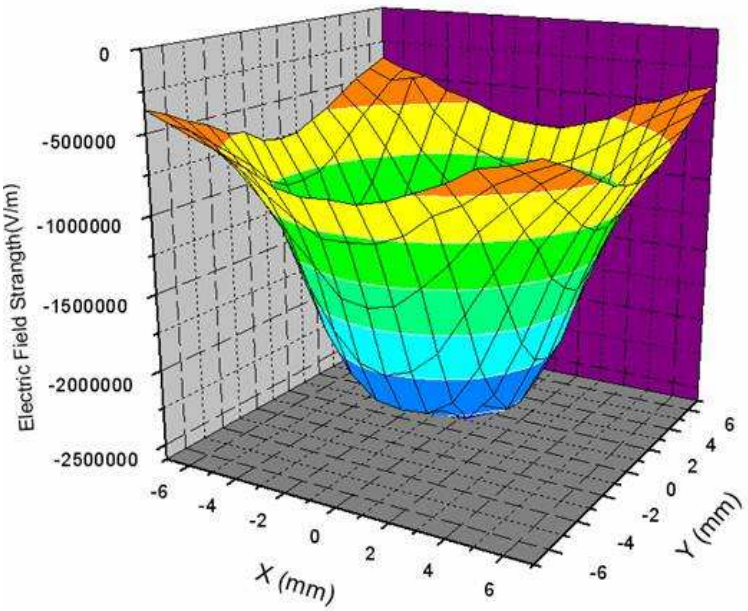

Figure 4-13(c) Matrix calculation of Type III lens at Line 1 (Fixed Z axial; 0.1mm to substrate)

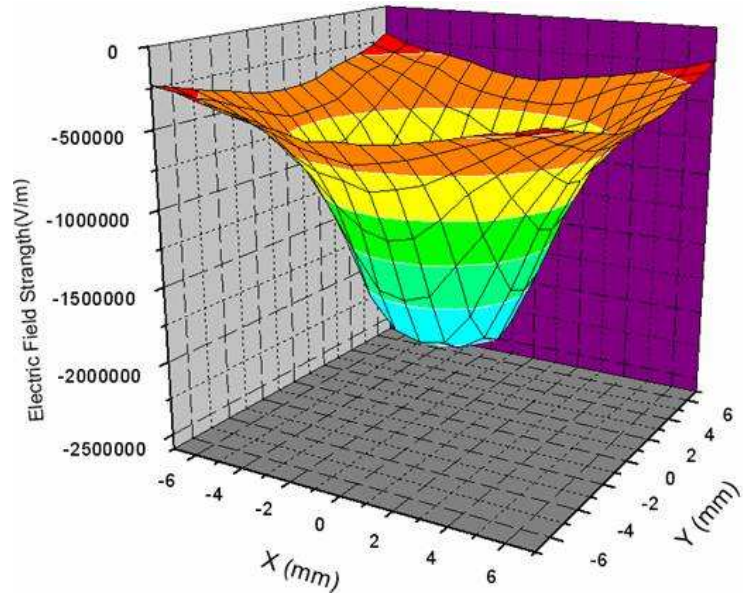

Figure 4-13(d) Matrix calculation of Type IV lens at Line 1 (Fixed Z axial; 0.1mm to substrate)

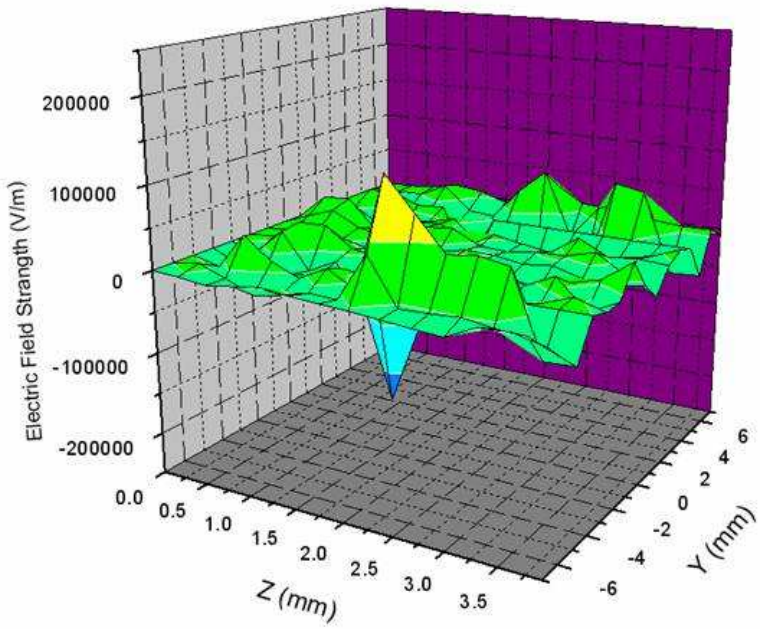

Figure 4-14(a) Matrix calculation of Type I lens (Fixed X axial)

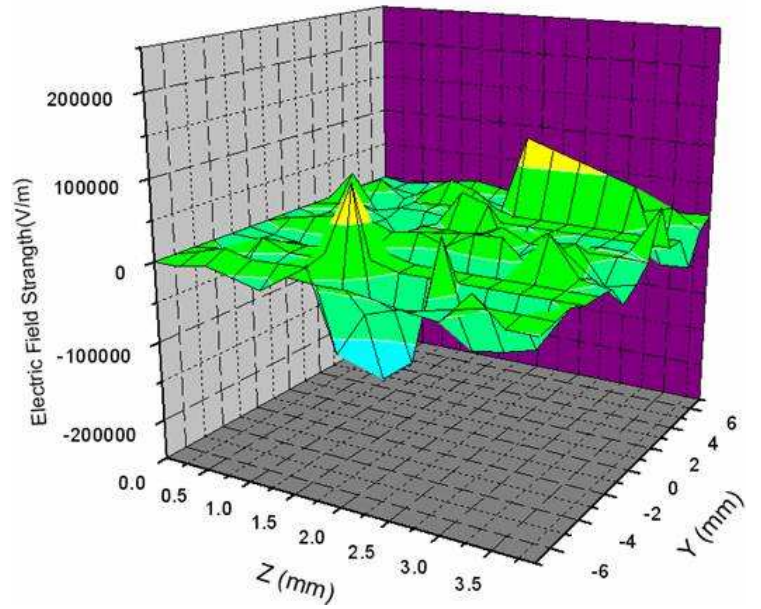

Figure 4-14(b) Matrix calculation of Type II lens (Fixed X axial)

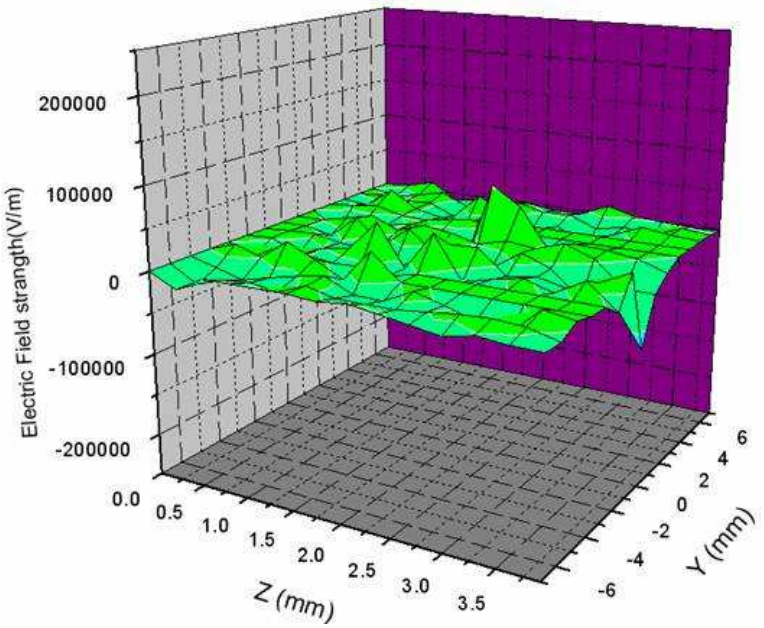

Figure 4-14(c) Matrix calculation of Type III lens (Fixed X axial)

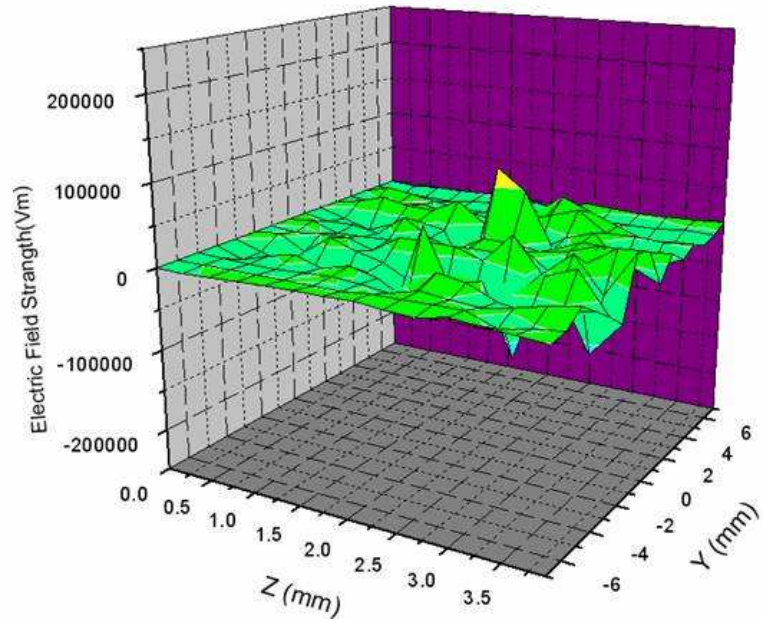

Figure 4-14(c) Matrix calculation of Type III lens (Fixed X axial)

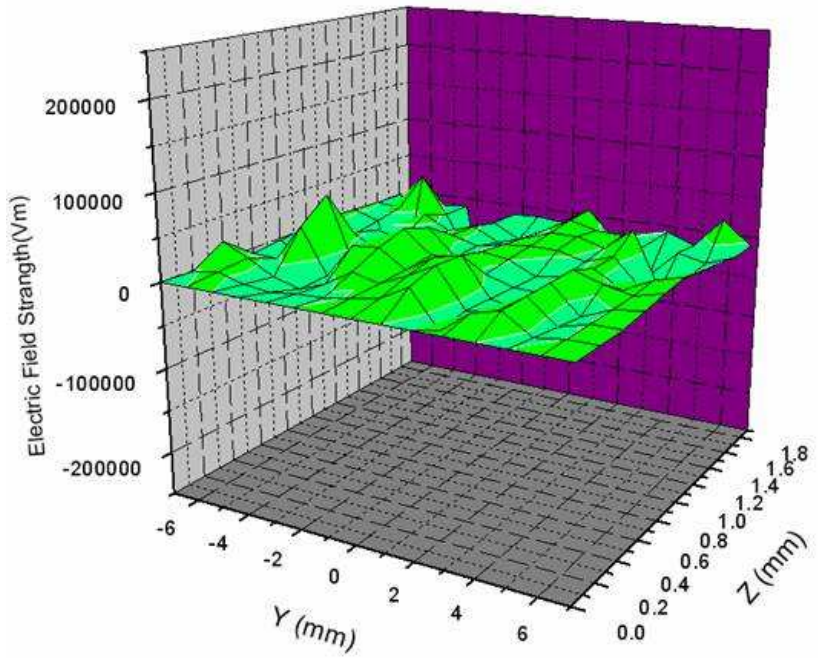

Figure 4-15(a) Matrix calculation of Type I lens (Fixed X axial)

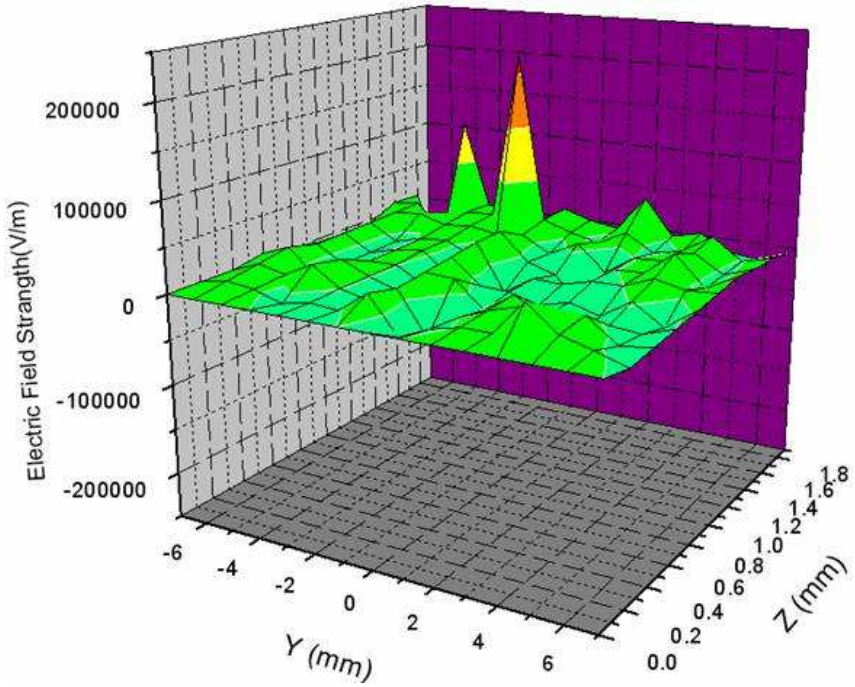

Figure 4-15(b) Matrix calculation of Type II lens (Fixed X axial)

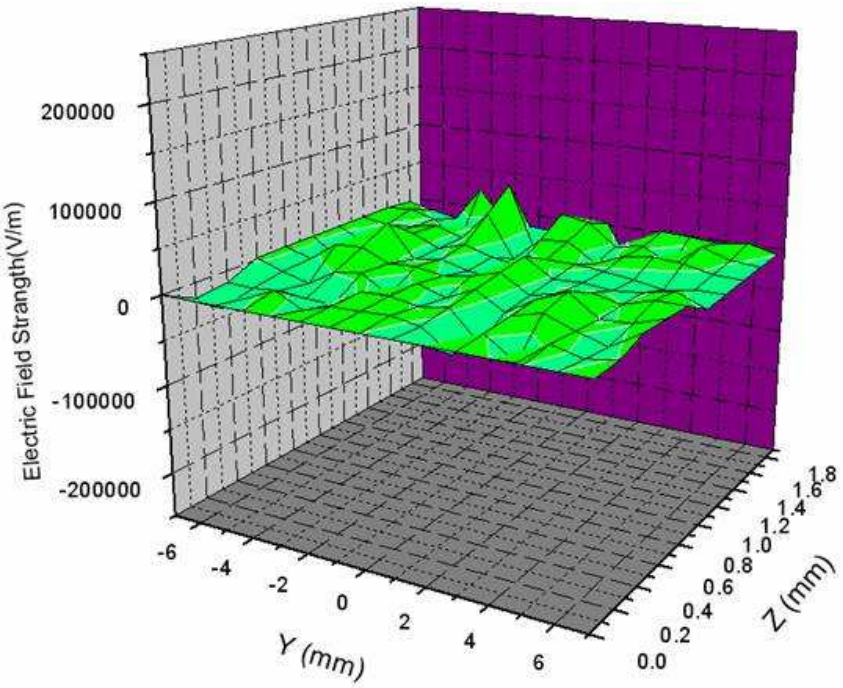

Figure 4-15(c) Matrix calculation of Type III lens (Fixed X axial)

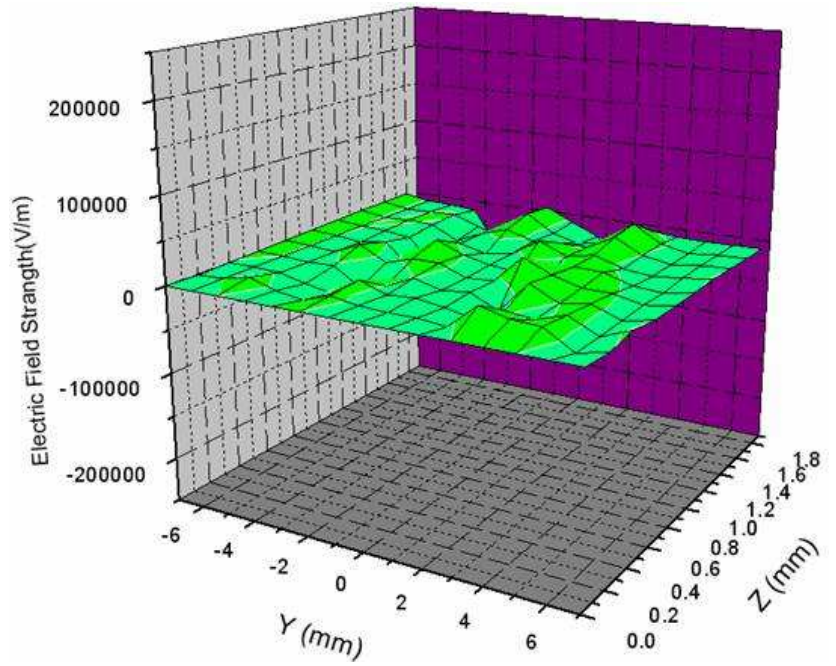

Figure 4-15(d) Matrix calculation of Type IV lens (Fixed X axial)

5. Patterning of EHD nanocolloid jet by using the EHD lens

5.1 Experimental setting

System

The experimental setup consisted of a liquid supply system, an electrical system, and a moving stage system. The liquid supply system included a syringe pump (minimum flow rate: 16.7 pl/min for 1ml syringe) and a stainless steel nozzle (inner diameter: 180 μm, outer diameter: 360 μm). A silver nanoparticle suspension was injected downward from the nozzle. The moving stage system consisted of an X-Y moving stage and a digital control system, in which a programmable motion-controller that communicated directly with a PC controlled the motion of a substrate. The electrical system consisted of a high voltage power supply (~DC 15kV) and two electrodes. The nozzle used for the liquid supply system was also used as an anode as well as an electrohydrodynamic lens, which was located 2.0 mm below the nozzle (Figure 5-1)

Figure 5-1 Experimental setting

Experimental Condition

Voltage	Flow rate	Substrate material
5.0 kV	1 μl/min	Photo paper

Material (Ink, Substrate)

Ink material : Cabot silver suspension

- Viscosity : 14.4 cP at 22˚C
- Solid loading : 20 wt%
- Carrier fluid : ethylene glycol

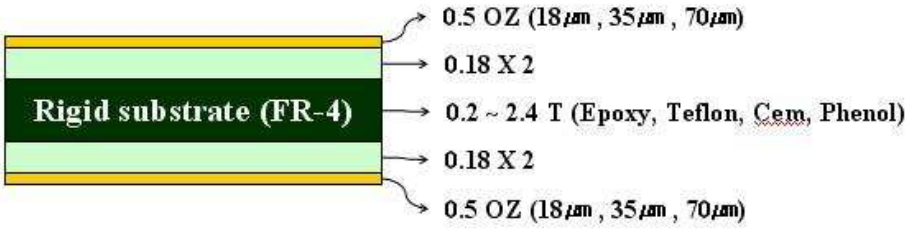

Figure 5-2 Diagram of Substrate (FR-4)

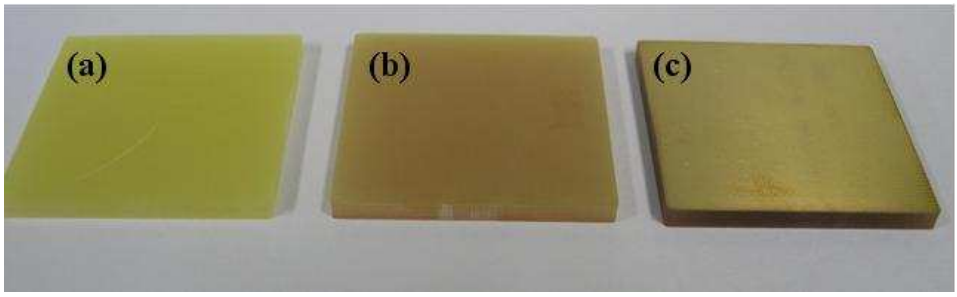

Figure 5-3 Substrate (FR-4) ; (a)without coating of Cu, (b)One-side coating of Cu, (c)Double-faced coating of Cu

5.2 Results

Figure 5-4 shows patterns obtained by using the Type II and Type III lens. The pattern widths were about 100 µm and 80 µm when the type II and III were used, respectively. The result shows that patterns with lower width were generated when the Type III was used. Figure 5-5 shows patterns obtain at FR-4 substrate and compare fabricate lens material Aluminum to Brass. This patterning is to use one-side of Cu coating FR-4 Rigid substrate. Figure 5-6 shows patterns obtain at FR-4 rigid substrate This substrate is without Cu coating. Figure 5-7 show pattern obtain at Double-faced FR-4. Consequently, Pin-Lens type of electrohydrodynamic system proves to possible electrohydrodynamic nanocolloid jet printing and Lens do a role between electrode and guide ring at Pin-Pin type.

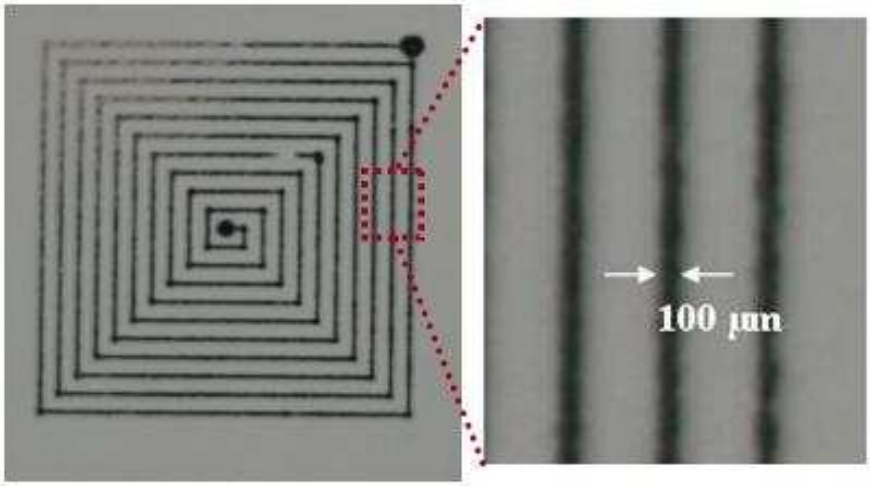

Figure 5-4(a) Pattern result of Type II lens (Photo paper)

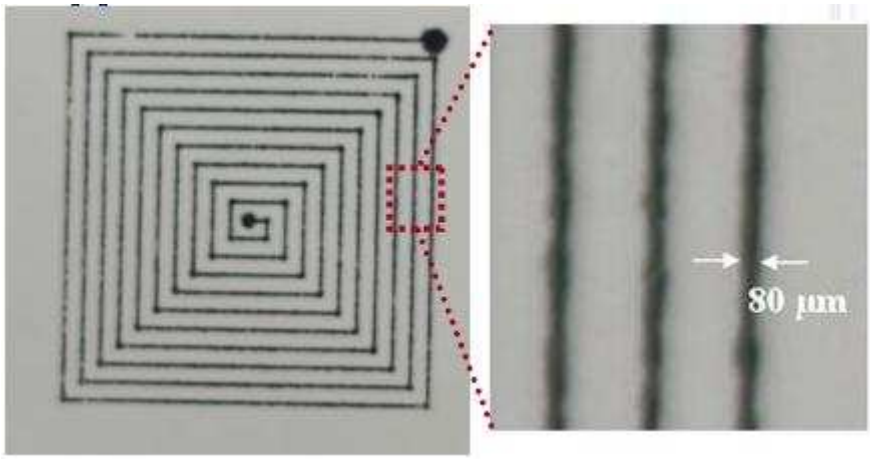

Figure 5-4(b) Pattern result of Type III lens (Photo paper)

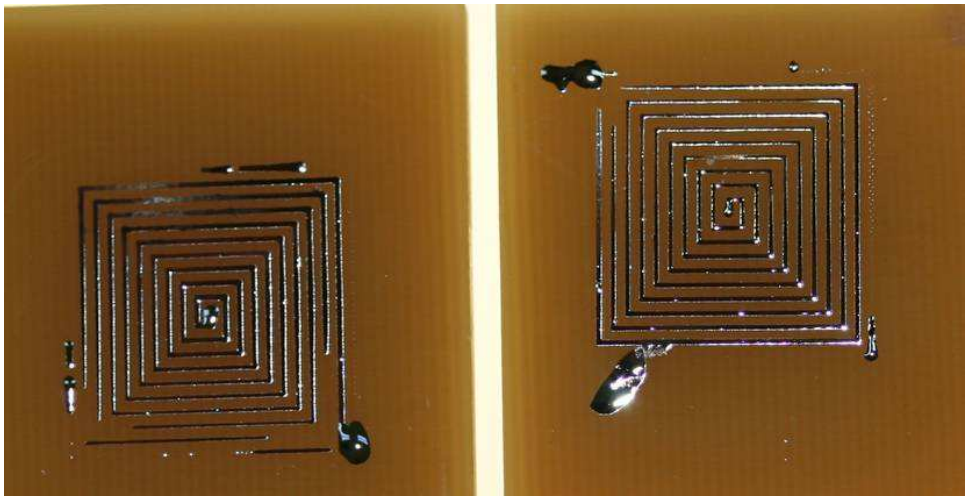

Figure 5-5 Comparison of pattern result by using Type I lens

(FR4; One-side coating of Cu)

; Aluminum Lens (left), Brass Lens (Right)

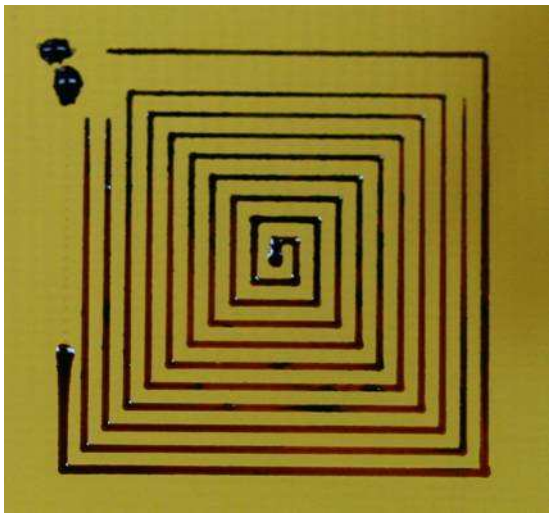

Figure 5-6 Pattern result by using Type I lens
(FR4; without coating of Cu)

Figure 5-7 Pattern result by using Type I lens
(FR4; Double-faced coating of Cu)

6. Discussion & Conclusion

Patterns of silver nanoparticles were obtained by using the various electrohydrodynamic lenses in electrohydrodynamic printing. The pattern width measured by using the Type I lens was about 150 μm. When the Type II and III were used, the pattern widths measured were about 100 μm and 80 μm. When the Type IV lens was used, the simulation results showed that the electric field strength was concentrated near the center of the lens and thus narrow electric fields were generated at the end of the lens. Pin-Lens type of electrohydrodynamic system proves to possible electrohydrodynamic nanocolloid jet printing and Lens do a role between electrode and guide ring at Pin-Pin type.

As previously explained, the more electric field strength is higher, the more repulsive force is higher. Because Type IV lens is to generate highest electric field strength, radial force of outside effect is very little. Data of Each line gained by the Maxwell, as show likely physical modeling result, which arrange by Origin as form of Matrix 3-dimension.. Because low rough of graph face is little effect of radial force, these graphs explain about stabilization.

▪ Reference

Barrero, A., Gañán-Calvo, A.M., and Fernandez-Feria, R. (1996), The Role of Liquid Viscostiry and Electrical Conductivity on the Motions inside Taylor Cones in E.H.D. *Spraying of Liquids, Journal of Aerosol Science*, Suppl. I. S175-S176

Calvert, P. (2001), Inkjet printing for materials and devices, *Chemistry of Materials*, 13, 3299-3305

Castro, T., Reifenberger, R., Choi, E., and Andres, R. P. (1990), Size-dependent Melting Temperature of Individual Nanometer-Sized Clusters, *Physical Review B*, 42, 13, 8548-8556.

Chen, C. –H., Saville, D. A., and Aksay, I. A. (2006), Scaling Laws for Pulsed Electrohydrodynamic Drop Formation, *Applied Physics Letters*, 89, 124103.

Chen, D. –R., Pui, D. Y. H., and Kaufman, S. L. (1995), Electrospraying of Conducting Liquids for Monidisperse Aerosol Generation in the 4 nm to 1.8 μm Diameter Range, *Journal of Aerosol Science*, 26, 963-977.

Chen, D. –R., and Pui, D. Y. H. (1997), Experimental Investigation of Scaling Laws for Electrospraying: Dielectric Constant Effect, Aerosol Science and Technology, 27, 367-380.

Chrisey, D. B. (2000), Materials Processing – the Power Direct Writing, *Science*, 289, 879-881.

Cloupeau, M., and Prunet-Foch, B. (1989), Electrostatic Spraying of Liquids in Cone-jet Mode, *Journal of Electrostatics*, 22, 139-159.

Calvert, P. D., Patra, P. K., Warner, S. B., and Fan, Q. (2004), Nano-Crafted Layered Optical Filaments for Diffractive Colors, *NTC Annual Report*, NTC Project No; M03-MD14.

Cottet, D., Grzyb, J., Kirstein, T. and Tröster, G. (2003), Electrical Characterization of Textile Transmission Lines, *IEEE Transaction on Advanced Packaging*, 26, 2, 182-190.

Fernández de la Mora, J., Navascues, J., Fernandez, F., and Rosell-Llompart, J. (1990) Generation of Submicron Monodisperse Aerosols in Electrospray, *Journal of Aerosol Science*, 21, special issue, S673-S676

Fernández de la Mora, J., and Loscertales, I. G. (1994), The Current Emitted by Highly Conducting Taylor Cones, *Journal of Fluid Mechanics*, 260, 155-184.

Gañán-Calvo, A. M., Davila, J., and Barrero, A. (1994), The Emitted Current and Droplet Size Laws and Steady Cone-Jet Electrosprays of Polar and Non-polar Liquids, *Proceedings of the Fourth International Aerosol Conference*, Los Angeles, CA. August 29 – September 2.

Gañán-Calvo, A. M., Davila, J., and Barrero, A. (1997), Current and Droplet Size in the Electrospraying of Liquids. Scaling Laws, *Journal of Aerosol Science*, 29, 2, 249-275.

Gomez, A., and Tang, K. (1991), Characterization of Low Flow Rate High Charge Density Electrosprays, *Proceedings of the Fifth International Conference on Liquid Atomization and Spray Systems*, ICLASS-91 (H. Semerjian, ed.), NIST(National Institute of Standards and

Technology) Special Publication, 83, Gaithersburg. MD, 771-778

Gomez, A., and Tang, K. (1994) Charge and Fission of Droplets in Electrostatic Sprays, *Phys. Fluid*, 6, 404-414.

Hartman, R. P. A., Brunner, D. J., Camelot, D. M. A., Marijnissen, J. C. M., and B. Scarlett. (2000), Jet Break-up Electrohydrodynamic Atomization in The Cone-jet Mode, *Journal of Aerosol Science*, 31, 1, 65-95.

Hayati, I., Bailey, A. I., and Tadros, Th. F. (1986), Mechanism of Stable Jet Formation in Electrohydrodynamic Atomization, *Nature*, 319, 41-43.

Jayasinghe, S. N., Edirisinghe, M. J., and Wilde, T. D. (2002), A Novel Ceramic Printing Technique Based on Electrostatic Atomization of a Suspension, *Materials Research Innovations*, 6, 92-95.

Jayasinghe, S. N., Edirisinghe, M. J. (2004), Electrostatic Atomisation of Ceramic Suspension, *Journal of European Ceramic Society*, 24, 2203-2213.

Kim, H. S., Lee, K. H., and Kim, S, G. (2006), Growth of Monidisperse Silver Nanoparticles in Polymer Matrix by Spray Pyrolysis, *Aerosol Science and Technology*, 40, 536-544.

Lee, D. Y., Hwang, E. S., Yu, T. U., Kim, Y. J., and Hwang, J. (2006), Structuring of Micro Line Conductor Using Electro-hydrodynamic Printing of a Silver Nanoparticle Suspension, *Applied Physics. A*, 80, 671-674.

Lee, D. Y., Yu, J. H., Yu, Y. U., and Hwang, J. (2006), Effect of Pin Diameter on Ceramic Nanoparticle Patterns Formed by Electro-

Hydrodynamic Printing with Pin-to-Pin Electrodes, *Journal of Electrostatics*, submitted.

Lee D. Y., Lee J. C., Shin Y. S., Park S. E., Yu T.U & Hwang J.H., "Patterning Conductive Silver Line by electrohydrodynamic Deposition and its electrical characterization", Journal of physics:conference series, 2007. 9(Accepted for publication at September)

Lee D. Y., Shin Y. S., Park S. E., Yu T. U & Hwang J. H., "Electrohydrodynamic Priniting of Silver Nanoparticles by using a Focused Nano-Colloid Jet", Applied Physics Letters, 90, 081905, 2007

Lefebvre, A. H. (1989), Atomization and Sprays, *Hemisphere Publishing Coporation*, Chap. 2, pp.37-39.

Li. J. L. (2006), On the Meniscus Deformation When Pulsed Voltage is Applied, *Journal of Electrostatics*, 64, 1, 44-52.

Loscertales, I. G., and Fernandez de la Mora, J. (1993), Characterization of Electrospray Generated Nanoparticles in a Hypersonic Impactor, *Journal of Aerosol Science*, 27, 695-720.

Lord Rayleigh (1878), On the Instability of Jets, *Proceedings of London Mathematical Society*, 10, 4-13.

Lord Rayleigh (1882), On the Equilibrium of Liquid Conducting Masses Charged with Electricity, *Philosophical Magazine*, Ser. 5. 184-186.

Nobaru, I., Yoshiharu, O., and Seiichiro, K. (1998), *Introduction to Ultrafine Particles(Jap.)*, Ohmu, Tokyo.

Pique, A., and Cheisey, D. B. (2002), *Direct Write Technologies for Rapid*

Prototyping Applications, Academic Press, San Diego.

Poon, H. F, (2002), *Electrohydrodynamic Printing*, Ph. D. Thesis, Department of Chemical Engineering : Princeton University.

Shin Y. S., Lee D. Y., Kim S. Y., Park S. E., Yu J. H., Yu T. U & Hwang J. H., "Design of Electrohydrodynamic Lens for stabilizing of electrohydrodynamic printing", Journal of physics: conference series, 2007 (Accepted for publication at September)

Tang, K., and Gomez, A. (1995), Generation of Monodisperse Water droplets from Electrosprays in a Corona-Assisted Con-Jet Mode, *Journal of Colloid and Interface Science*, 175, 326-332.

Taylor, G. I. (1964), Disintegration of Water drops in an Electric Field. *Proceedings of Royal Society*, A 280, 383-397.

Vonnegut, B., and Neubauer, R. L. (1952), Production of Monodisperse Liquid Particles by Electrical Atomization, *Journal of Colloid Science*, 7, 616.

Yu, J. H., Lee, D. Y., and Hwang. J. (2006), Effect of Variation in Electrode Diameter and Flow Rate on Formation of Pattern by Electrohydrodynamic Spraying, *Proceedings of the Seventh International Aerosol Conference*, 627-628.

Yu, J. H., Lee, D. Y., Hwang, E. S., Yu, T. U., Kim, Y. J., and Hwang, J. (2005), 은 나노 입자 프린팅을 이용한 마이크로 전도성 라인 형성에 관한 연구, *Proceedings of KAPAR Conference*, 247-248.

Zeleny, J. (1914), The Electrical Discharge from Liquid Points, and a Hydrostatic Method of Measuring the Electric Intensity at Their

Surfaces, *Physical Review*, 3, 2, 69-91.

Zeleny, J. (1915), On the Conditions of Instability of Electrified Drops with Applications to the Electrical Discharge from Liquid Points. *Proceeding of Cambridge Philosophical Society*. 18, 71-83.

Zeleny, J. (1917), Instability of Electrified Liquid Surfaces, *Physical Review*, 10, 1, 1-6.

▪ **Summary in Korean (국문요약)**

은 나노콜로이드 젯을 이용한 전기수력학 프린팅의 안정성을 위한 전기수력학 렌즈의 설계 및 응용에 관한 연구

직접쓰기 기술을 통해서 마이크로 패터닝을 만들어 내는 기술이 요즘 화두로 떠오르고 있으며 다양한 기술의 발전들이 이루어지고 있다. 그 중에서도 가장 많은 관심을 가지고 있는 기술이 잉크젯 기술이며 잉크젯 기술을 통해서 다양한 물질들을 기판 위에 직접 프린팅을 하여 원하는 모양이나 글씨 및 인덕터, 전도성 라인들을 원하는 모양대로 적은 잉크를 사용하면서 만들어 내는 기술들이 연구되고 있는 상황이다. 리소그래피와 같은 첨단장비들을 이용하는 기술이 현재 산업용으로 사용되고 있지만, 많은 소재들을 낭비하는 등의 친환경적이지 못한 부분과 작은 선폭을 가진 도선들을 표현할 수 있지만 너무 많은 단계의 공정이 필요하여 간단하고 단순한 공정단계를 가진 직접쓰기 기술이 대두되고 있는 것이다. 이에 전기수력학 방법을 통한 직접쓰기 기술의 핵심인 헤드기술을 연구함에 있어 프린팅 기술의 안정성 및 정확성을 향상시키기 위한 것에 그 목적이 있다고 할 수 있다. 그동안 핀-핀 타입의 형태로 노즐과 기판 밑에 전극핀, 기판과 노즐 사이에 가이드링이 있는 형태로 다양한 연구가 진행되어 왔지만, 다음과 같은 세 가지 정도의 문제점을 보게 되었다.

(1) 노즐과 기판 아래에 있는 전극 핀의 일직선으로 맞추기가 쉽지 않다.

(2) 전극이 기판 아래에 있어 기판이 전도성을 띄거나, 두꺼우면 그 기판 아래 전극을 사용할 수 없게 되어 프린팅을 할 수 없다.

(3) 기판과 기판 아래의 전극핀 사이의 간격이 너무 좁아, 노즐과 기판과의 위치를 움직이는데 용이하지 못하다.

이와 같은 단점을 보완해서 가이드링과 기판아래의 전극을 합치는 렌즈의 개념을 생각하게 되었고 핀-렌즈 타입 형태의 실험이 성공적으로 이루어지게 되어, 렌즈의 형태를 다양하게 변화시켜가며 안정적인 프린팅 방법을 연구하게 되었다. 기판아래 전극핀이 없어지게 됨으로 인해 전도성을 가진 기판이나 두꺼운 기판에도 프린팅을 할 수 있게 되었으며, 노즐과 렌즈만 중심을 맞추면 되기 때문에 보다 쉽게 동심도를 맞출 수 있게 되었다. 또한 기판과 노즐과의 거리를 자유롭게 움직일 수 있어 앞에서 얘기한 세 가지의 단점을 보완하는 기술을 개발했다고 할 수 있다. 네 가지 형태의 렌즈를 우선 맥스웰과 컴솔 프로그램으로 어떤 것이 더 효율성과 안정성 등이 좋은지 모사해보고 각각의 렌즈를 직접 제작하여 프린팅 실험을 하여 비교해 보았다. 그 결과 렌즈의 내부의 형태변화를 통해서 일정부분 모아지는 효과를 볼 수는 있었지만 외부의 두께 조절을 통해서는 더 많은 효과를 기대할 수 없었다. 이에 외부의 모양을 변화시키게 되면 좀더 안정성이 향상 된 렌즈를 설계할 수 있을 것으로 보인다.